

DEACTIVATION AND REGENERATION OF IMMOBILIZED TITANIUM DIOXIDE  
PHOTOCATALYSTS DURING TREATMENT OF PHARMACEUTICAL MICROPOLLUTANTS IN  
GROUNDWATER

BY

ZACHARY SASNOW

THESIS

Submitted in partial fulfillment of the requirements  
for the degree of Master of Science in Environmental Engineering in Civil Engineering  
in the Graduate College of the  
University of Illinois at Urbana-Champaign, 2014

Urbana, Illinois

Adviser:

Associate Professor Timothy J. Strathmann

## ABSTRACT

As detection methods improve, a number of classes of emerging contaminants are being detected in natural waters, including many pharmaceuticals and personal care products (PPCPs). Many of these chemicals are recalcitrant to conventional treatment processes, so new treatment methods are being investigated. Titanium dioxide (TiO<sub>2</sub>)-based photocatalytic treatment has proven to be an effective method for degrading trace organic contaminants, including PPCPs. However, most studies on photocatalytic treatment of PPCPs to date have been conducted in short-term batch experiments using fresh catalysts in laboratory solutions devoid of non-target constituents that are often abundant in natural water matrices (e.g., Ca<sup>2+</sup>, HCO<sub>3</sub><sup>-</sup>, natural organic matter). In this contribution, we describe the results of an investigation of the long-term stability and deactivation of immobilized TiO<sub>2</sub> photocatalysts used to treat PPCPs in groundwater (GW). GW spiked with four model PPCPs (5 µg/L atenolol, sulfamethoxazole, carbamazepine, and 10 µg/L iopromide) was treated with immobilized thin films of TiO<sub>2</sub> coated on glass slides under UV-A light in a serpentine plug-flow reactor. Initially, catalysts achieved 50-75% degradation of influent PPCPs using a 2-hr reactor residence time (higher removal can be achieved using longer residence times). Over one month of continuous operation, catalyst films developed visual discoloration and the extent of PPCP removal in the reactor diminished, eventually reaching complete catalyst deactivation for some of the target PPCPs. Calcite (CaCO<sub>3(s)</sub>) with smaller quantities of iron and copper were detected on the surface of deactivated catalyst films when analyzed by scanning electron microscopy coupled with energy-dispersive X-ray spectroscopy (SEM-EDS), X-ray diffraction (XRD), and X-ray photoelectron spectroscopy (XPS). Treatment of deactivated catalysts with 10 mM hydrochloric acid was able to restore catalyst activity to pre-GW levels, so introduction of recurrent acid washing stages during GW treatment were investigated to prolong catalyst activity. Pretreatment of GW using a sodium-loaded cation exchange softening resins was investigated to eliminate calcite precipitation in the reactor. Although calcite precipitation was eliminated, catalysts continued to experience a similar loss of activity observed for unsoftened GW. Analysis of catalyst surfaces after exposure to softened groundwater indicates deposits of zinc, copper, iron, and manganese. Results suggest that both physical blocking of active sites by calcite surface precipitates and adsorption of trace metals contribute to catalyst deactivation. Further work is needed to investigate other pretreatment methods such as pH modification to prevent surface deposition of catalyst-deactivating metal species on the TiO<sub>2</sub> surface and prolong reactor activity between acid washing regeneration stages.

## **ACKNOWLEDGEMENTS**

This work was supported by a National Science Foundation CAREER Award to T. Strathmann (CBET 07-46453) and the Global Collaborative Research Office of King Abdullah University of Science and Technology (KAUST) through the Collaborative Research on Sustainable Water Development and Engineering Partnership. Materials characterization was carried out in part in the Frederick Seitz Materials Research Laboratory Central Facilities, University of Illinois. I would like to thank Dr. Timothy Strathmann for his guidance both in my undergraduate and graduate research work. I also would like to thank Sean Carbonaro, Matthew Sugihara, and Laura Asmuth for their design and construction of the titanium dioxide catalyst preparation method, dipcoating apparatus, and flow-through reactor. I would also like to thank Raul Tenorio for his help with several analytical methods; I would also like to thank Raul Tenorio, Mengwei Han, and Yalin Li for their help with occasional sample collection, Linda Holyoke for use of her algorithm to calculate photon flux from spectroradiometer data, and Dr. Shaoying Qi for his help with general laboratory tasks and analytical work.

## TABLE OF CONTENTS

1. INTRODUCTION .....	1
2. EXPERIMENTAL METHODS.....	4
2.1. Reagents and Supplies .....	4
2.2. Titanium Dioxide Photocatalyst .....	4
2.3. Plug-Flow Reactor .....	4
2.4. Continuous-Flow Micropollutant Treatment Experiments .....	5
2.5. Target PPCP Compounds .....	5
2.6. Catalyst Characterization.....	6
2.7. Catalyst Treatments & Batch Treatment Experiments.....	6
2.8. Analytical.....	6
2.9. Tables and Figures .....	8
3. RESULTS AND DISCUSSION .....	10
3.1. Catalyst, Reactor, and Groundwater Characterization.....	10
3.2. Long-Term PPCP Treatment in Buffered DI Matrix .....	10
3.3. Long-Term PPCP Treatment in Groundwater Matrix .....	11
3.4. Chemical Treatment and Regeneration of Deactivated Catalyst Films .....	14
3.5. Long-Term Groundwater Exposure with Recurrent Chemical Treatment.....	15
3.6. Pre-Treatment of Groundwater by Softening.....	15
3.7. Tables and Figures .....	17
4. CONCLUSIONS .....	34
5. REFERENCES .....	35

## 1. INTRODUCTION

Advancements in medicine and chemistry over the last century have undoubtedly improved the quality of life for many around the world. In particular, many synthetic pharmaceuticals have been introduced to treat human and veterinary diseases and improve livestock productivity. However, the fate of these compounds in environmental systems is often unknown or disregarded during the course of their use, and as a result many pharmaceutically active compounds have entered into the natural environment. This emerging class of contaminants, collectively called pharmaceuticals and personal care products (PPCPs), includes such synthetic chemicals such as pharmaceuticals, illicit drugs, veterinary medications, cosmetics, sunscreen ingredients, fragrances, and food additives. Developments in analytical techniques in recent decades have allowed the detection of these compounds at the trace concentration they are typically present at (ng/L to µg/L) in environment. As a result, PPCPs have been detected in a growing number of surface and groundwaters throughout the United States and other parts of the world<sup>1-3</sup>.

PPCPs have a wide variety of routes through which they can enter the natural environment. A common route is through the excretion of pharmaceuticals not used by the body, or the dumping of unused medications into household plumbing, moving the PPCPs into the wastewater stream. Though the concentrations of these compounds in natural matrices are typically low, the effect of chronic exposure to low concentrations remains largely unknown. The toxicity of many PPCPs and their effects on non-target receptors in the body is not fully understood, as well as any synergistic effects PPCPs present together in mixtures.<sup>1</sup> There has been evidence of some PPCPs acting as endocrine disruptors in marine ecosystems and causing sexual disruption in fish.<sup>4</sup> There is also concern for the accumulation of PPCPs in recycled wastewater used for direct or indirect potable reuse applications,<sup>5</sup> groundwater recharge,<sup>6</sup> or accumulation in soils irrigated with recycled wastewater.<sup>7</sup> Many people rely on groundwater as their major source of potable water, and PPCPs have been detected in many groundwater sources.<sup>8-10</sup> PPCPs are not currently regulated as drinking water contaminants in the United States, but some PPCPs have begun to appear on the EPA's Contaminant Candidate List (CCL) indicating priority interest and potential for future regulation.

The growing presence of PPCPs in surface and groundwater results in them often being present in source waters used by drinking water treatment plants. Treated wastewater used in groundwater recharge can introduce PPCPs into groundwater as wastewater treatment plants are not specifically designed to remove PPCPs and other trace organic pollutants, and therefore many PPCPs can pass through treatment plants intact or only partially eliminated.<sup>6,11,12</sup> Conventional wastewater treatment processes are not effective for the removal of many of these compounds; activated sludge and ozonation have been shown to degrade some PPCPs, though often not to more than 1-log removal. Other PPCPs are recalcitrant toward these processes, and are only partially or not removed during wastewater treatment.<sup>13,14</sup>

Advanced oxidation processes (AOPs) are a group of technologies that show promise in addressing trace organic pollutants like PPCPs. AOPs generate hydroxyl radicals ( $\cdot\text{OH}$ ), a strong non-selective oxidant that reacts with most all organics. AOPs encompass several technologies including ozonation, UV/O<sub>3</sub>, UV/H<sub>2</sub>O<sub>2</sub>, and some

photocatalytic processes.<sup>15</sup> Titanium dioxide (TiO<sub>2</sub>) photocatalysis has shown promise for treatment of a number of PPCPs.<sup>16-19</sup> TiO<sub>2</sub> is activated by UV light at energies exceeding the material's semiconductor bandgap energy ( $\lambda < 400$  nm and 384 nm for rutile and anatase crystalline TiO<sub>2</sub> phases, respectively), exciting valence band electrons to the conduction band ( $e_{cb}^-$ ) and leaving behind strongly oxidizing valence band holes ( $h_{vb}^+$ ). In water, the  $e_{cb}^-$  can then react with adsorbed O<sub>2</sub> to form superoxide radicals (O<sub>2</sub><sup>-</sup>) or react with other electron-accepting species (e.g., organohalogen contaminants), whereas the  $h_{vb}^+$  can react with organic contaminants directly or react indirectly by reacting with adsorbed hydroxide and water molecules to form ·OH, which can then react with the target contaminant at near diffusion-limited rates. TiO<sub>2</sub> is inexpensive and biologically inert in most systems.<sup>20,21</sup> There is also potential to use solar irradiation to activate TiO<sub>2</sub> photocatalysts,<sup>22</sup> and research efforts are underway to modify TiO<sub>2</sub> materials to expand the wavelength range for photo-excitation.<sup>23</sup> TiO<sub>2</sub> photocatalysis, both in UV and visible light, has been shown to deactivate microorganisms as well as deactivate pharmaceutically and toxicologically active compounds.<sup>17,18,24,25</sup>

Although TiO<sub>2</sub> photocatalysis shows promise as a treatment technology for PPCP-contaminated water sources, a number of critical issues need to be addressed before effective pilot studies can be performed and scaled up designs put into practice. First, greater understanding of long-term catalyst performance in real water matrices is needed. Natural waters contain dissolved minerals and natural organic matter at concentrations that are several orders of magnitude higher than PPCPs and other target contaminants. These substances can interact with catalyst surfaces and react with  $e_{cb}^-$ ,  $h_{vb}^+$ , and ·OH, thereby inhibiting reactions with target PPCPs or deactivating the catalysts. Some studies have reported on the effects of common non-target constituents, but the applicability of findings to treatment applications is often obscured because the concentration of PPCPs used in the experiments were much higher than the actual concentrations present in natural waters (many times the added PPCPs are even the major source of organic carbon in the experimental solutions, which is not the case under real-world conditions where non-target substances are the major scavengers of reactive species<sup>26,27</sup>). In addition, the TiO<sub>2</sub> catalyst is typically studied as suspensions or slurries of TiO<sub>2</sub> nanoparticles, and tests are typically performed only as short-term batch experiments.<sup>28</sup> These conditions do not accurately reflect conditions that would be encountered in real engineered treatment systems where catalysts will most likely be immobilized on larger support structures to facilitate material separation from the water, and catalysts will be exposed to a continuous feed of sourcewater containing both target contaminants and non-target constituents. Studies done with immobilized TiO<sub>2</sub> photocatalyst in deionized water matrices show substantial catalyst activity, indicating promise for this method of photocatalyst preparation.<sup>29</sup>

To address these issues, we have designed a reactor system to measure the effect of non-target constituents on TiO<sub>2</sub> photocatalysts. Previous work done by Carbonaro *et al.*<sup>30</sup> developed a serpentine plug-flow reactor wherein TiO<sub>2</sub> thin films were immobilized on horizontal glass supports lining the bottom of the reactor flow path and irradiated with commercial UV-A light sources (centered at  $\lambda = 365$  nm). This reactor was designed with the intent of investigating various factors that will affect the stability of TiO<sub>2</sub> photocatalysts during treatment and indicate their potential for regeneration during long-term treatment applications. The reactor system was used initially to study

continuous treatment of PPCPs present in tertiary treated wastewater effluent. Photocatalytic treatment of PPCPs was inhibited in the wastewater effluent matrix during continuous treatment experiments conducted for periods of up to 1 week (acetaminophen = 40% inhibition; carbamazepine = 60%; iopromide = 78%; sulfamethoxazole = 54%). Much of the inhibition was reversible when the wastewater matrix was removed and replaced by a comparable pH-buffered deionized water matrix, suggesting that non-target constituents in the wastewater inhibit by scavenging of photocatalyst-generated reactants or reversibly adsorbing and blocking reactive sites. At the same time, a portion of the decrease in activity was not recovered upon removal of the wastewater matrix, indicating non-target organic and inorganic constituents also contribute to photocatalyst deactivation. The work also highlighted the need for studies in other relevant sourcewater matrices as well as the need to extend studies for longer periods of time (>1 week) to assess the progression of deactivation processes, identify mechanisms responsible for inhibition and deactivation, and investigate the potential for reversing deactivation by targeted surface chemical cleaning processes.

This contribution builds upon the work of Carbonaro and coworkers,<sup>30</sup> describing the effects of long-term continuous treatment of PPCP-contaminated GW. Deactivation of the photocatalyst thin films was observed after long-term exposure to groundwater (>1 month). Deactivated catalysts were characterized by a suite of microscopic and spectroscopic techniques to identify causative agents and mechanisms responsible for catalyst deactivation, and this information was used as the basis for chemical cleaning strategies for restoring catalyst activity. Recurrent chemical treatments were incorporated into longer-term (multiple month) continuous operation of the reactor. The effects of pre-treating groundwater by softening to prevent operation of surface deactivation mechanisms were also evaluated.

## 2. EXPERIMENTAL METHODS

### 2.1. REAGENTS AND SUPPLIES

All chemicals used were reagent grade and obtained from Fisher Scientific or Sigma-Aldrich unless otherwise noted. Iopromide was provided by Schering AG (Berlin, Germany) as a gift. Nanophase titanium dioxide was provided by Degussa (Type P25, 50 m<sup>2</sup> g<sup>-1</sup>; mixture of anatase and rutile).<sup>31</sup> GW samples were obtained from a well drawing water from beneath Newmark Civil Engineering Building at the University of Illinois (Urbana, IL). Prior to use, GW was aerated overnight for at least 12 h to oxidatively precipitate dissolve iron and manganese and then filtered sequentially with 10 μm and 1 μm membrane filters (Polygard-CR 10 μm and Lifegard 1 μm, Millipore), unless otherwise indicated, and stored under darkness at 4 °C. Sodium-loaded softening ion exchange resins (model FC024) were obtained from Pure Water Products, LLC. Deionized (DI) water was used to prepare all other solutions (Barnstead NANOpure systems; >17.5 MΩ·cm resistivity). **Table 2.1** provides a full listing of reagents used in this study.

### 2.2. TITANIUM DIOXIDE PHOTOCATALYST

Immobilized thin films of TiO<sub>2</sub> photocatalysts were prepared using procedures previously described.<sup>30</sup> Briefly, glass microscope slides with dimensions of 75 mm × 25 mm × 1 mm (Thermo Scientific Gold Seal) were dip coated in a sol-gel composed of 30 g/L TiO<sub>2</sub> nanoparticles mixed into a gel containing 0.42 M titanium isopropoxide, 1.68 M diethanolamine, and 0.84 M water in isopropanol. An automated dip-coating apparatus was used to lift microscope slides in and out of the sol-gel at a controlled rate of 20 cm/min. Dip-coated slides were then dried at room temperature for 24 h before calcining in a programmable furnace. Heating was conducted in several steps; first heating to 100 °C at 3 °C/min, holding for 1 h, increasing to 600 °C at the same rate, holding for 1 h, and then cooling to ambient temperature. The dip-coating process was done three times; previous tests indicated no significant increase in catalytic activity with additional coats.<sup>30</sup>

### 2.3. PLUG-FLOW REACTOR

The serpentine plug-flow reactor used in this work was described previously;<sup>30</sup> diagrams and photographs of the reactor are shown in **Figure 2.1**. The reactor is divided into five channels, each lined with glass slides containing immobilized thin film TiO<sub>2</sub> photocatalysts. Catalyst films and the overlying solution were irradiated with UV-A lamps (General Electric F15T8, 15W, irradiance centered at λ = 365 nm) suspended above each of the five channels at a height of 12 cm. Flow depth in the reactor was controlled by a 0.62 cm weir at the effluent end of the reactor channel, with a total reactor volume of 325 mL. Flow was controlled by a Masterflex L/S digital standard drive peristaltic pump. Water was pumped into and out of the reactor using Masterflex silicone tubing; the tubing uses proprietary sizing. The inlet tubing was Masterflex size 13 and the outlet tubing was size 14; outlet tubing was slightly larger to allow complete removal of effluent water from the spillover point and to prevent any over-accumulation of effluent. A total reactor residence time of 2 h was set by controlling the flowrate at 2.7 mL/min, and



was verified by perchlorate tracer test. This residence time was selected to achieve no more than 90% degradation of the target pharmaceutical compounds used in the study to enable better assessment of changes in catalyst activity over time. Although complete removal of the target PPCPs could be achieved by altering reactor residence times, the reactor was not designed with the intent of developing a larger scale reactor for field applications, but rather to serve as a bench-scale system for studying factors controlling long-term activity and deactivation of photocatalysts in different water matrices.

#### 2.4. CONTINUOUS-FLOW MICROPOLLUTANT TREATMENT EXPERIMENTS

Continuous-flow experiments were conducted to examine the effects of long-term exposures to GW on the activity of photocatalyst thin films for treating PPCPs. UV lamps were warmed up for >1 h prior to beginning an experiment. Influent matrices were prepared in 20 L glass containers connected to the inlet tubing of the peristaltic pump; the reactor was filled to volume (325 mL) with the influent matrix prior to turning on the pump and beginning the experiment. Sample aliquots were collected at the end of the fourth reactor channel. This sampling location was selected (rather than the reactor effluent) to allow for occasional removal and replacement of individual catalyst film slides before the sample point for analysis without reducing the total number of catalyst films before the sampling point (slides located downstream from the sampling point were moved upstream when one was removed for interrogation). The residence time at that point was estimated to be 80% of the full reactor residence time, or 96 min. Samples were collected every 10 min for the first 2 h of each experiment to show the reaching of steady-state conditions in the reactor; otherwise samples were taken at intervals sufficiently exceeding that of the hydraulic residence time to ensure no disturbance in reactor conditions from collection of 3 mL samples. Similarly, after switching between solution matrices [e.g., buffered deionized water (DI) to GW], a sample was not collected for several reactor residence times in order to ensure steady state conditions were achieved again. Influent matrices were switched cyclically between buffered DI water, GW, and an acid cleaning solution containing 10 mM HCl. The buffered DI water matrices were prepared by adding NaHCO<sub>3</sub> and adjusting the pH with HCl and NaOH to match the pH and alkalinity of the GW samples used in the same experiment.

#### 2.5. TARGET PPCP COMPOUNDS

Target PPCP compounds (**Table 2.2**), encompassing a variety of uses and structures, were selected based on their recalcitrance to conventional water and wastewater treatment technologies.<sup>13</sup> A mixed stock solution of the target PPCPs was added to reactor influent matrices (buffered DI or GW) to achieve the corresponding initial concentration (5 µg/L for ATN, SMX, and CBZ; 10 µg/L for IOP due to lower sensitivity of the analytical method) sufficient to enable direct detection by liquid chromatography-tandem mass spectrometry (LC-MS/MS) without need for sample pre-concentration steps. Although this concentration is higher than typical values for PPCPs measured in natural waters (i.e., < 1 µg/L), it is orders of magnitude lower than the concentrations of important non-target constituents including natural organic matter (mg/L levels) and therefore is expected to behave as a trace component of the matrix. Previous tests showed similar reactivity of PPCPs in the reactor using an influent

concentration of 50  $\mu\text{g/L}$ , indicating concentration-independent behavior as trace constituents at conditions used in the study.<sup>30</sup>

## 2.6. CATALYST CHARACTERIZATION

Virgin, GW-deactivated, and acid-washed photocatalyst films were extensively characterized using a suite of techniques. Scanning electron microscope (SEM) images of catalyst surfaces were collected using a JEOL JSM-6060LV microscope, and energy dispersive X-ray spectra (EDS) of selected locations within the SEM images were collected using an Oxford Instruments ISIS EDS system connected to the microscope. Samples were sputter coated with Au/Pd prior to analysis in SEM-EDS. X-ray diffraction (XRD) analysis was conducted using a Panalytic/Philips X'Pert MRD system using Cu  $K\alpha$  radiation. Sample coupons were attached to glass microscope slides with transparent tape and fixed onto the sample platform using more tape. Crystalline phases were compared to the Powder Diffraction File (PDF) database for identification. X-ray photoelectron spectroscopy (XPS) was conducted using a Kratos Axis Ultra XPS system. Catalyst samples were loaded into an anoxic sample chamber on carbon tape. Raman spectroscopy was conducted using a Nanophoton Raman 11 Laser Raman microscope. A laser wavelength of 523 nm and grating of  $1400\text{ cm}^{-1}$  was used for Raman analysis at  $10\times$  magnification.

## 2.7. CATALYST TREATMENTS & BATCH TREATMENT EXPERIMENTS

Testing of chemical cleaning treatments for catalyst regeneration was performed using small batch treatments prior to the introduction of a treatment method into the flow-through reactor. Individual catalyst films or coupons of catalyst films (made by scoring individual catalyst films with a diamond-tip scribe and breaking along the score line) were placed in a 300 mL Berzelius beaker. A stir bar in the beaker was placed under a perforated plastic platform for the catalyst to allow stirring without contact between the catalyst and stir bar. Treatments lasted for 24 h. Chemical treatments in the flow-through reactor, such as acid washing, were conducted by introducing the treatment chemical into the reactor in the same fashion as the GW/buffered DI experiments. Flow rates and all other physical characteristics of the reactor setup remained the same. Chemical treatments lasted 24 h.

## 2.8. ANALYTICAL

PPCP concentrations were determined by LC-MS/MS analysis after filtration (0.22  $\mu\text{m}$  cellulose acetate) using an Agilent 1200 Series LC with electrospray ionization (ESI) and an Agilent LC/MSD Trap XCT Ultra mass spectrometer. Two HPLC methods were used over the course of the study, each having different stationary and mobile phases. One method used a Zorbax Eclipse XDB-C18 column ( $4.6 \times 150\text{ mm}$ , 5  $\mu\text{m}$  particle size) as the stationary phase and a gradient mobile phase at 0.2 mL/min composed of two solvents (A: 95% water, 5% acetonitrile, and 0.1% formic acid; B: 95% acetonitrile, 5% water, 0.1% formic acid). After sample injection, solvent B was held at 0% for five min, then increased to 90% over the next 12 min, then increased to 100% over the next min, then held at 100% for 4 min before decreasing to 0% over the next 2 min and holding for 6 min. The second method used a Zorbax Eclipse XDB-C18 column ( $2.1 \times 100\text{ mm}$ , 3.5  $\mu\text{m}$  particle size) as the stationary phase and a gradient mobile phase at 0.2 mL/min composed of two solvents (A: 95% water, 5% methanol, and 0.1% formic acid;

B: 95% methanol, 5% water, and 0.1% formic acid). After sample injection, solvent B was increased to 75% over 5 min, then increasing to 100% over the next 1 min, held at 100% for 4 min, then decreased to 0% over the next 3 min and held at 0% for 7 min. For both methods target PPCPs were quantified against external standards by monitoring the following positive ion mass transitions and fragmentation voltages (potential differences between skimmer and capillary exit): ATN (267→145 m/z, 89.8 V), IOP (92→573 m/z, 99.5 V), SMX (254→156 m/z, 82.6 V), CBZ (237→194 m/z, 84.7 V). The quantification limit for ATN, SMX, and CBZ was approximately 0.5 µg/L, and for IOP the quantification limit was approximately 1 µg/L.

Perchlorate used in reactor tracer tests was quantified by ion chromatography analysis with conductivity detection (IC-CD; Dionex ICS-2000, 100 µL sample loop, Dionex IonPac AS16 column, 36 mM KOH eluent, 1 mL/min flow rate). GW was analyzed for bulk and trace constituents. Anions in GW samples ( $\text{SO}_4^{2-}$ ,  $\text{PO}_4^{3-}$ ,  $\text{NO}_3^-$ ,  $\text{F}^-$ ,  $\text{Cl}^-$ ,  $\text{Br}^-$ ) were also analyzed by IC-CD with Dionex IonPac AS19 Column (Dionex ICS-2000, 100 µL sample loop, 1 mL/min flow rate) with a gradient eluent method (10 mM KOH for 0-10 min, 10-45 mM linear increase of KOH from 10-25 min, hold at 10 mM KOH from 25-30 min). Elemental analysis was conducted using inductively coupled plasma-mass spectrometry (ICP-MS; Perkin Elmer Sciex Elen DRCE). Dissolved organic carbon (DOC) was analyzed using a Shimadzu TOC-VCPH combustion analyzer. Other water quality parameters (pH, alkalinity) were determined using the *Standard Methods for the Examination of Water and Wastewater*.<sup>32</sup> UV bulb irradiance spectra were collected using an International Light Technologies ILT950 spectroradiometer.

## 2.9. TABLES AND FIGURES

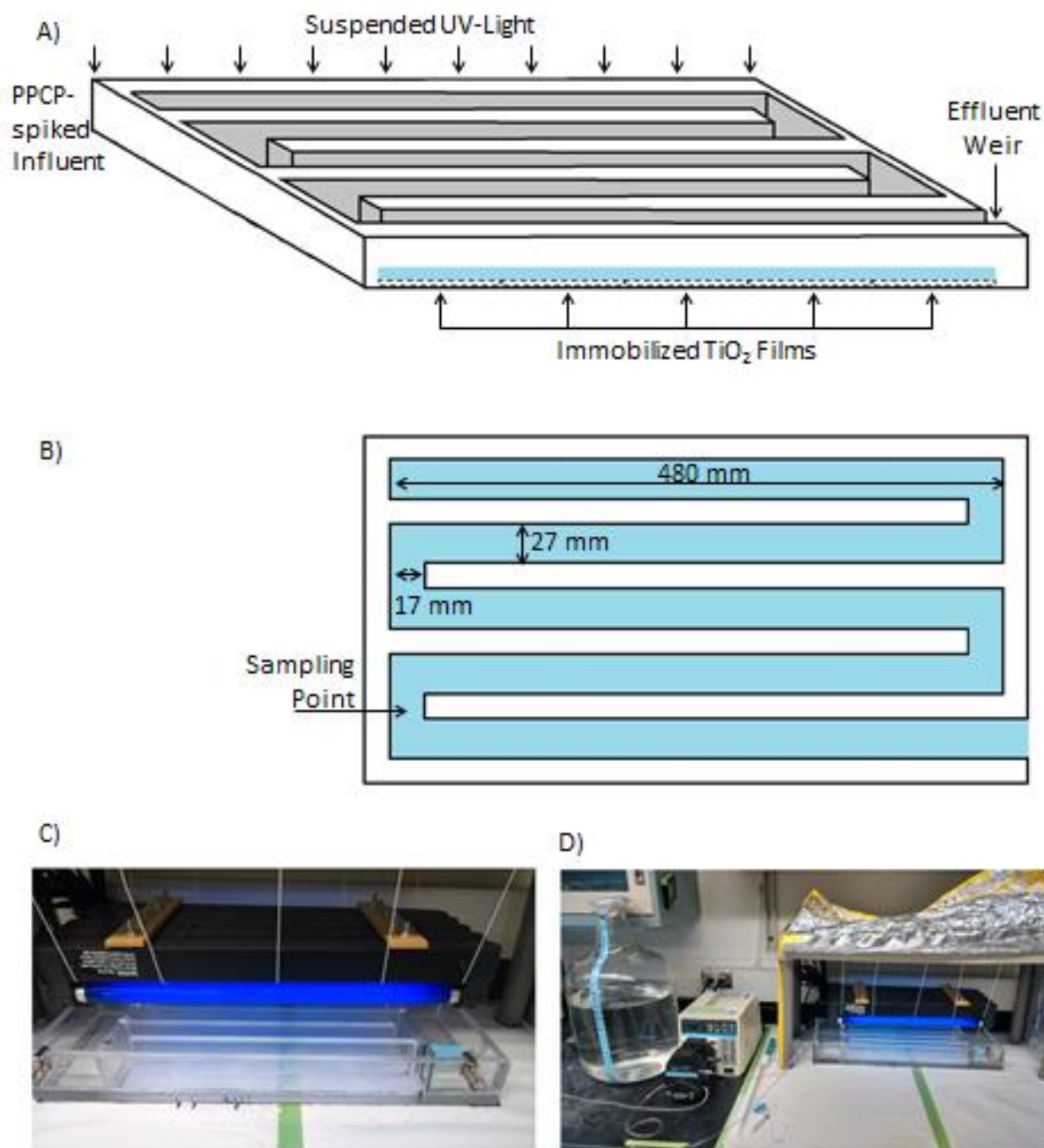


**Figure 2.1: Diagrams and images of plug-flow reactor used in this study. A) 3-dimensional drawing of reactor with inlet and outlet labels. B) Overhead diagram view of reactor with width and length dimensions and sampling point location. C) Close-up view of reactor under suspended UV lights. D) View of experimental setup, including inlet reservoir, peristaltic pump, and reactor setup.**

Reagent	Supplier	Purity	Use
Atenolol	Sigma-Aldrich	≥97%	Analytical PPCP
Iopromide	Schering AG	Not Specified (Gift)	Analytical PPCP
Sulfamethoxazole	Sigma-Aldrich	99%	Analytical PPCP
Carbamazepine	Sigma-Aldrich	≥99%	Analytical PPCP
Titanium Isopropoxide	Sigma-Aldrich	99.999%	TiO <sub>2</sub> sol-gel
Titanium Dioxide	Degussa	≥99.5%	TiO <sub>2</sub> sol-gel
Isopropanol	Fisher Scientific	99.9%	TiO <sub>2</sub> sol-gel
Diethanolamine	Sigma-Aldrich	99%	TiO <sub>2</sub> sol-gel
Acetonitrile	EMD Millipore	>99.8 (HPLC grade)	HPLC mobile phase
Methanol	Fisher Scientific	99.9%	HPLC mobile phase
Formic Acid	Sigma-Aldrich	~98%	LC/MS proton source
Sodium Bicarbonate	Fisher Scientific	>99.9%	Buffer for buffered DI matrix
Hydrochloric Acid	Sigma-Aldrich	99.9%	Acidifying groundwater/acid rinsing reactor
Sodium Perchlorate	Sigma-Aldrich	>98.0%	Tracer test

Table 2.1: Reagents used in this study.

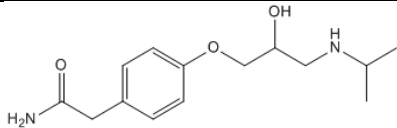
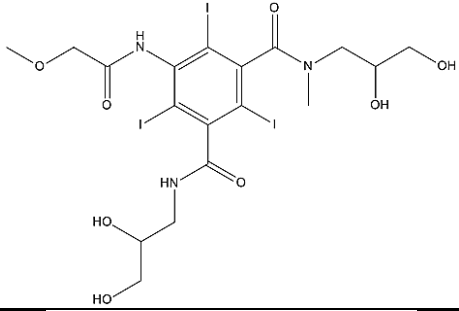
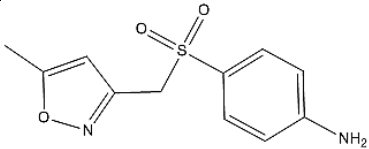
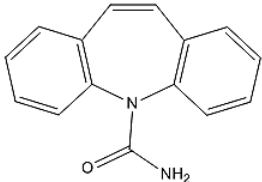
Compound	Abbreviation	Structure	Molecular Weight (g mol <sup>-1</sup> )	Use
Atenolol	ATN		266.3	β-blocker
Iopromide	IOP		791.1	X-ray contrast agent
Sulfamethoxazole	SMX		253.3	Antibiotic
Carbamazepine	CBZ		236.3	Anticonvulsant

Table 2.2: List of target PPCP compounds used in this study.

### 3. RESULTS AND DISCUSSION

#### 3.1. CATALYST, REACTOR, AND GROUNDWATER CHARACTERIZATION

Catalyst thin films were prepared using procedures described by Carbonaro and *et al.*,<sup>30</sup> and virgin films exhibited similar properties.<sup>30</sup> **Figure 3.1** shows SEM images and associated EDS spectra, **Figure 3.2** the XRD spectrum, **Figure 3.3** the Raman spectrum, and **Figure 3.4** the XPS spectrum of the virgin catalyst surface. Results were similar to those found by Carbonaro and coworkers.<sup>30</sup> XRD data indicate a distribution of TiO<sub>2</sub> crystalline phases in the film to be 91.5% anatase and 8.4% rutile, consistent with earlier reports of Degussa P25 being a mixture of the two phases.<sup>31</sup> Raman spectra also show a strong signal from anatase, and a small contribution from amorphous silica that is attributed to the underlying glass substrate. As expected for unadulterated TiO<sub>2</sub>, XPS characterization indicates major contributions to the surface chemistry from Ti and O.

The hydraulic and irradiance properties of the plug flow reactor were also characterized. **Figure 3.5** shows the results of a perchlorate tracer test conducted in the reactor, resulting in a characteristic mean residence time of 1.90±0.13 h when operating with a flowrate of 2.7 mL/min, close to the reactor's theoretical residence time of 2.0 h corresponding to a liquid filled volume of 325 mL. **Figure 3.6** shows a plot of the averaged irradiance spectrum of the UV-A lamps collected at 30 different points in the reactor flowpath 12 cm below the lamps (same distance as the thin films). The centroid of this spectrum is located at  $\lambda = 360.5$  nm, near the manufacturer's specification of 365 nm. The photon flux incident on the catalyst surface, calculated from the spectroradiometer data, is  $4.94 \times 10^{-9}$  E s<sup>-1</sup> cm<sup>-2</sup>.

**Table 3.1** lists the characteristics of the buffered DI and groundwater matrices used in this study. It should be noted that the measured dissolved organic carbon (DOC = 1.52 mg/L) is significantly higher than the dissolved carbon concentration of the target PPCPs added to the influent matrix (~10<sup>3</sup> times higher by mass), as intended. The source groundwater used in this study has an average alkalinity of 217.7 mg/L as CaCO<sub>3</sub>, and contains significant calcium (34 mg/L), magnesium (24 mg/L), sodium (23 mg/L), and beryllium (14 mg/L). There are also lesser quantities of silicon, lithium, potassium, barium, zinc, copper, manganese, chloride, nitrate, sulfate, fluoride, phosphate, and bromide. Given the pH of the influent groundwater (8.46), it is expected that significant bicarbonate ion is present.

Using a solubility product for calcite of  $3.36 \times 10^{-9}$ ,<sup>33</sup> and calculating the carbonate concentration from the measured alkalinity and pH, the groundwater is supersaturated with respect to calcite ( $[\text{Ca}^{2+}][\text{CO}_3^{2-}] = 2.30 \times 10^{-8}$ ). Assuming activity coefficients of 1.0 for calcium and carbonate, the saturation index (SI) is 0.84. Therefore, precipitation of calcite is favorable.

#### 3.2. LONG-TERM PPCP TREATMENT IN BUFFERED DI MATRIX

**Figure 3.7** shows the results from a long-term control experiment assessing the photocatalytic treatment of the target PPCPs in the buffered DI water matrix. An influent matrix composed of 4.5 mM sodium bicarbonate

(NaHCO<sub>3</sub>) and the four model PPCP compounds in deionized water was treated in the reactor for 28 d. The concentration of sodium bicarbonate was chosen to give the control an alkalinity of 209 mg/L as CaCO<sub>3</sub> and pH of 8.41, which is comparable to the GW matrices used in other experiments (**Table 3.1**). **Figure 3.7** shows that catalyst activity for the four model compounds after 28 d of exposure to the buffered deionized matrix fluctuated over time, but did not show an increasing trend toward initial concentrations, which would indicate a loss in catalyst activity. Variance in the data is attributed to the low influent concentrations of the model compounds used, and the sensitivity of the analytical method used for analysis. The analytical method was subsequently changed to improve the stability of measurements at conditions used in the study. After approximately 1.5-2 h (the hydraulic residence time of the reactor at the sampling point being approximately 96 min) the activity reached a steady state for the four model compounds.

These results demonstrate the stable activity and structure of the immobilized TiO<sub>2</sub> thin films over extended periods of time when exposed to a “clean” influent stream devoid of the myriad of non-target constituents present in natural water matrices. It follows that changes in catalyst activity and structure observed for long-term treatment of PPCPs in GW can be attributed to catalyst interactions with non-target constituents present in the GW rather than matrix-independent deactivation mechanisms.

### 3.3. LONG-TERM PPCP TREATMENT IN GROUNDWATER MATRIX

**Figure 3.8** shows the timecourse data for long-term groundwater exposure in the reactor. The experiment began with 3 d of PPCP treatment in buffered DI matrix to establish a stable baseline of activity, followed by 30 d of treatment in the GW matrix, followed by 3 d of treatment again in the buffered DI matrix. **Table 3.1** lists the major characteristics of the buffered DI and groundwater matrices.

The level of treatment for individual PPCPs in the initial buffered DI phase of the experiment were consistent with results from the long-term control experiment reported in **Figure 3.7**. The levels of treatment for the four target compounds in the initial buffered DI treatment phase were as follows: ATN: 62±5% removal, IOP: 55±8%, SMX 79±2%, CBZ: 59±5%. Upon switching to the GW matrix, the extent of PPCP treatment decreased. Initial removal in GW was less than removal in buffered DI, but the magnitude of the difference varied for individual target compounds; for ATN activity decreased by 35% (62±5% in buffered DI to 40±4% for the first 3 d of GW treatment), for IOP 49% (55±8% to 28±9%), for SMX 27% (79±2% to 58±4%), and for CBZ 42% (59±5% to 34±5%). This initial loss of apparent catalyst activity after switching to GW is generally lower than that reported by Carbonaro *et al.* when switching from buffered DI to a tertiary-treated wastewater effluent (WWE) matrix, though similarly to that study the loss of activity was observed immediately upon switching matrices, indicating some catalyst inhibition by dissolved constituents in the matrix such as natural organic matter (NOM).<sup>30</sup> The alkalinity of the WWE used by Carbonaro *et al.* was 104 mg/L as CaCO<sub>3</sub>,<sup>30</sup> approximately half of the GW used in this study, indicating that carbonate species alone are not responsible for the relative loss of catalyst activity seen in WWE and GW matrices. Reversible inhibition can result from non-target constituents competing with the PPCPs for adsorption to catalyst surfaces and reaction with reactive species generated at the catalyst-water interface (e.g.,

·OH). This is consistent with other studies showing GW matrices causing less catalyst inhibition than WWE matrices, attributed to the higher NOM content of typical WWE than the GW matrix used in this study, and potentially other radical scavenging substances.<sup>34</sup>

Results show that over the 30 d GW matrix exposure, catalyst reactivity with the target PPCPs was progressively lost, leading to complete deactivation for some target compounds. Treatment of IOP and CBZ decreased to the greatest extent, with complete loss of any treatment following 10-12 d of continuous treatment. IOP decreased from 28±9% average removal on the first three days of GW treatment to complete deactivation by day 10. CBZ decreased from 34±5% average removal on the first three days of GW treatment to complete deactivation by day 12. In contrast, only partial deactivation was observed for SMX, with average removal decreasing from an initial value of 58±4% during the first three days to 33±4% after 30 d of continuous treatment. The slower relative loss of activity could be attributed to SMX reactivity with carbonate radicals that form in alkaline groundwater matrices in addition to hydroxyl radicals.<sup>19</sup> Aniline moieties such as that present in the SMX structure have been shown to be very reactive with carbonate radicals,<sup>35</sup> and previous studies have shown that increasing bicarbonate concentration has an enhancing effect on SMX degradation by TiO<sub>2</sub>.<sup>19</sup> ATN lost most activity by the end of the groundwater exposure, decreasing from 40±4% removal on the first day of GW treatment to 15±4% removal at the end of the GW treatment phase; the residual level of activity may also be due to its documented reactivity with carbonate radicals.<sup>36</sup> ATN has been reported to be more reactive to carbonate radicals than CBZ, but less reactive than SMX.<sup>36</sup> Studies have shown that increasing bicarbonate concentration in natural river water enhanced TiO<sub>2</sub> photocatalytic activity with respect to ATN degradation.<sup>16</sup> Data collected from the three days of buffered DI after the GW treatment phase show a small amount of recovery in activity for SMX and ATN, but reactivity did not return to levels observed in the initial buffered DI treatment phase. This suggests some reversible matrix-derived inhibition of the catalyst activity, but most of the observed loss in treatment in GW was irreversible and likely due to accumulation of catalyst poisons and foulants from the GW matrix onto the surface of the TiO<sub>2</sub> films during long-term exposure. **Figure 3.9** presents the averaged pseudo-first order rate constants for both buffered DI exposures (only points after steady state conditions were reached for the first exposure were used) as well as the last three days of GW exposure.

Exposure to the GW matrix resulted in a brown discoloration of the catalyst films (**Figure 3.10**), with more intense discoloration occurring closer to the reactor inlet. This suggests surface deposition of trace constituents is responsible for the discoloration (bulk components whose concentration remain relatively unchanged throughout the reactor would cause more uniform discoloration). **Figure 3.11** shows the SEM-EDS results of the catalyst surface after deactivation compared to the virgin catalyst surface. Compared to the virgin catalysts, the deactivated catalysts were covered in crystalline deposits; EDS analysis of the surface deposits show a strong signal for calcium ions in the deposits. XRD data (**Figure 3.12**) show the presence of calcite (CaCO<sub>3</sub>(s)); this is consistent with the alkaline nature of the groundwater matrix and the supersaturated conditions noted previously. **Figure 3.13** shows XPS spectra of the deactivated catalyst surface. The presence of Ca and CO<sub>3</sub><sup>2-</sup> peaks are consistent with the presence of calcite deposits as well. Comparison between the XPS spectral range for C between the virgin (**Figure 3.13d**) versus



deactivated catalysts show the presence of C 1s peaks in the latter corresponding to both adventitious C (sample support tape) as well as an additional C peak at 289 eV consistent with carbonate ions in calcite surface deposits.<sup>37</sup> XPS analysis also indicates the presence of small peaks for both Cu and Fe, the latter being consistent with the brown discoloration observed (**Figure 3.13e**). **Table 3.2** lists the relevant characteristics of the GW matrix in the influent reservoir and in the collected effluent from the reactor. Interestingly, the concentration of calcium changes very little between the influent and effluent, suggesting only a small fraction of the dissolved calcium precipitates when passing through the reactor, yet with time this small amount accumulates to form the deposits observed. In contrast to Ca, Cu undergoes a significant reduction in concentration between the influent and effluent samples, supporting the XPS results suggesting co-deposition of Cu with calcite. Fe was actively removed from the GW matrix prior to use by aeration and filtration and was not detected in the influent GW samples used, but the metal's insolubility in oxidizing environments leads to accumulation of residual trace levels onto the catalyst surface that grow to detectable levels over the course of the 30 d treatment period.

As indicated in the initial analysis of the GW matrix, analysis of the GW matrix following 24 h of aeration and filtration (to oxidatively precipitate and remove Fe and Mn) indicates supersaturated conditions with respect to calcite. Prior to aeration, the pH of the GW is 7.77; under these conditions the SI is 0.15 (assuming similar alkalinity), only slightly supersaturated with respect to calcite. Aeration of the GW increases the pH by driving off excess carbon dioxide, raising the pH and shifting the dissolved carbonate speciation towards  $\text{CO}_3^{2-}$ , and raising the SI for calcite to 0.84. As indicated in **Table 3.2**, the pH of the effluent GW increases insignificantly (8.46 in influent to 8.52 in effluent), so the SI remains approximately constant in the GW through the reactor flowpath. Thus, the observed deactivation may be attributed, at least in part, to formation of calcite surface deposits that can block PPCP access to reactive sites, inhibit UV activation of the underlying  $\text{TiO}_2$  phases, or serve as centers of electron-hole pair recombination.

Given that pure calcite is white,<sup>38</sup> the brown discoloration indicates that other substances are also co-precipitating with the calcite, especially at the influent end of the reactor, which is supported by the presence of both Fe and Cu in the XPS spectrum of deactivated catalyst films with surface deposits present; in particular, the presence of Fe can explain the brown discoloration.<sup>38</sup> Elemental analysis of the aerated and filtered GW matrix (**Table 3.1**) shows detectable Cu, but not Fe. This suggests that Fe content in the GW after aeration and filtration is below the detection limit of the ICP-MS analysis (<1 ppt), yet still accumulates over time on the catalyst films to detectable levels. Studies have shown that  $\text{TiO}_2$  doped with various transition metals typically exhibit a reduction in their photocatalytic activity in the presence of these metals;<sup>39-41</sup> this effect could also explain the loss of activity of the photocatalyst after prolonged deposition of Fe and Cu with calcite on the surface along with physical blocking of the reactive surface from mineral deposits.

### 3.4. CHEMICAL TREATMENT AND REGENERATION OF DEACTIVATED CATALYST FILMS

Catalyst films from a previous experiment, which had been exposed to a similar groundwater matrix for 41 d, were used to test the efficacy of various chemical treatment methods to remove the deactivating surface deposits from the active porous TiO<sub>2</sub> films. Though calcite was identified as the primary material present in the surface deposits, a variety of chemical treatment methods, in addition to the obvious choice of acids to remove calcite, were investigated to explore which chemicals would effectively remove all deactivating material, including acids, bases, chelating agents, reducing agents, oxidizing agents, and surfactants. **Table 3.3** lists the chemicals surveyed. These were chosen to incorporate a multitude of chemical properties and reactivities. Treatment efficacies were assessed qualitatively using SEM-EDS analysis, comparing images and spectra of the treated catalyst coupons to deactivated catalyst and virgin catalyst surfaces. Of the treatment chemicals used, the disodium salt of EDTA and hydrochloric acid were the most effective at returning the films to a similar appearance as the virgin catalyst. For further chemical treatment work hydrochloric acid was used; it was chosen due to its faster reactivity than EDTA and its chemical simplicity. **Figure 3.14** shows the SEM-EDS comparison between the virgin and HCl-washed (10 mM, 24 h) catalyst films. Further studies will be needed to refine washing times and acid concentrations.

Using results from the chemical treatment screening experiment, a 24-h 10 mM hydrochloric acid washing feed was introduced into the reactor following 30 d of GW treatment (and subsequent 3 d of buffered DI water treatment). After the acid cleaning phase, buffered DI spiked with PPCPs was reintroduced into the reactor and treatment was monitored for an additional 3 d to assess the reversibility of the deactivation observed over the 30 d GW treatment experiment. **Figure 3.15** shows the results of this acid wash. The acid washing procedure largely recovered the catalyst activity to the levels observed prior to GW treatment. **Figure 3.16** shows the change in color of the catalysts in the reactor; the brown discoloration was removed and catalyst films returned to their initial white color. **Figure 3.17** shows a comparison between the SEM-EDS results of the virgin catalyst, deactivated catalyst, and acid washed catalyst surface. Surface deposits observed in the deactivated catalyst were removed following acid washing of the reactor and the catalyst films appeared to be similar in features to the virgin films. Acid dissolution of the calcite surface precipitates was supported by elimination of prominent Ca peaks in the EDS. Presumably, co-precipitated constituents contributing to the observed discoloration dissolve with the calcite upon acid treatment. These results suggest that the catalyst surface is not chemically altered significantly by the deactivating material, and deactivation can be attributed to physical blocking of the catalyst surface, or by an inhibitory effect from the transition metals (Fe, Cu) co-deposited with calcite on the surface that is reversed upon acid dissolution of these metals. These findings also suggest a general strategy for maintaining long-term activity of catalysts. Similar to membrane filtration processes, periodic chemical cleaning of catalysts can be used to recover lost activity and maintain design treatment levels.

### 3.5. LONG-TERM GROUNDWATER EXPOSURE WITH RECURRENT CHEMICAL TREATMENT

Using the information collected from the chemical treatment experiment, continuous treatment of the PPCPs was extended through several treatment and catalyst regeneration sequences to demonstrate longer-term reactor operation. After two weeks the GW treatment was followed by 24-h acid washing stages (10 mM HCl), identical to the previous acid wash done between buffered DI matrices. **Figure 3.18** shows the results of this recurrent cleaning step. As is most obvious with SMX and CBZ, the extent of activity loss between acid cleaning cycles is less than observed during the initial 30 d treatment cycle. It may be possible to further reduce the level of deactivation by increasing the frequency of acid washes (e.g., 1 h cleaning cycles every 24 h). Further studies are needed to optimize the washing sequence to maintain desirable levels of target contaminant treatment and minimize waste generation from the process. Following 3 GW treatment/acid washing cycles (42 d of treatment), the influent was switched back to the PPCP-spiked buffered DI feed. **Figure 3.19** compares the average pseudo-first order rate constants of the four three-day buffered DI matrix exposures; the activity slightly decreases at this point in the experiment. It was not tested whether or not this small loss in activity could have been reversed by modification of the washing procedure.

During the final acid wash, the entire acid flush water (4000 mL) was collected and dissolved solids were recovered by evaporation of the acid solution. Analysis of the resulting solids (**Table 3.4**) shows the presence of several cations, including Ca (presumably from calcite deposits), Mg, Na, and Si (possibly from the glass support as well as GW), and lesser amounts of other elements, including Cu, Fe, and Zn. Particularly of note is Fe, which was not detected above the detection limit in the influent GW matrix, but was detected in XPS of deactivated catalyst films.

### 3.6. PRE-TREATMENT OF GROUNDWATER BY SOFTENING

In addition to regenerative strategies for sustaining catalyst activity, pretreatment strategies can potentially be used to slow catalyst deactivation and extend the time period between required catalyst cleaning steps. A pretreatment strategy was examined to inhibit precipitation of calcite, the primary causative agent identified, by lowering the saturation index of the groundwater source. First, the effect of softening the GW matrix by ion exchange treatment was examined. After aerating the GW to promote oxidative precipitation of Fe and Mn, the GW was further pretreated by passing through a Na<sup>+</sup>-loaded commercial ion exchange softening resin (Pure Water Products LLC, FC024 cation exchange resin). **Table 3.5** shows major characteristics of the water before and after softening; passing the GW through the resin led to a substantial reduction in Ca<sup>2+</sup>, Mg<sup>2+</sup>, and most other major polyvalent cation species, with corresponding increase in Na<sup>+</sup> concentration. Note that softened GW used in this treatment was collected immediately beforehand, and is a different batch from the previous treatments in this study. Thus differences in characteristics are observed between the softened GW batch and previous GW matrices. Calculation of the SI of the GW after softening indicates the matrix was no longer supersaturated with respect to calcite (SI = -0.72).

Following the last acid wash after the exposure to groundwater with recurrent acid washes (Section 3.5), the reactor was returned to buffered DI for three days, followed by three weeks treating PPCPs added to the softened groundwater, before finishing the experiment with three days of treating PPCPs in the buffered DI matrix. **Figure 3.20** shows the results of this study. Surprisingly, the catalyst experienced similar deactivation throughout the course of this treatment, indicating that calcite precipitation is not the only factor causing deactivation of the catalysts. **Figure 3.21** shows the comparison of the rate constants from the previous groundwater study to the softened groundwater for the last three days of each exposure, as well as the intermittent buffered DI exposures; the softened GW inhibited the activity of the catalysts similarly to the unsoftened GW matrix despite the removal of calcite oversaturation conditions. **Figure 3.22** shows a comparison of the reactor after previous groundwater exposures to the reactor after softened groundwater exposure; a similar brown discoloration formed on the catalyst surface. The discoloration after the softened groundwater exposure is less intense than that after the first groundwater exposure, but this could be attributed to the extra week in the first groundwater exposure.

**Figure 3.23** shows SEM-EDS analysis of the deactivated catalyst surface compared to the virgin catalyst surface. SEM-EDS for both surfaces are very similar, and this method of analysis does not show any material on the catalyst surface that would indicate deactivation. Similarly to SEM-EDS, XRD does not show any deactivating material. **Figure 3.24** shows the XRD analysis of the catalyst surface at the end of the softened GW exposure. The XRD spectrum is virtually identical to the virgin catalyst spectrum as indicated in the figure. These results suggest that the deactivating material may be present in such small quantities and the  $\text{TiO}_2$  signals overwhelm the total signal, indicating the need for more surface-sensitive measurement such as XPS. XPS analysis of the surface (shown in **Figure 3.25**) indicates the presence of Zn and Cu, as well as trace signals from Fe and Mn; both the XPS and XRD results show no Ca as expected. These results suggest that the deactivating material is composed of a mixture of trace metals present in the groundwater that adsorb to the catalyst surface or precipitate on surfaces over the course of GW exposure. The XPS spectrum did not contain a shifted carbon peak at 289 eV, which would indicate carbonate precipitation. This may indicate that other anion species present in the matrix still promote precipitation, and that the presence of metals causing inhibitory effects to  $\text{TiO}_2$  photoactivity may be the primary cause of catalyst deactivation.

### 3.7. TABLES AND FIGURES

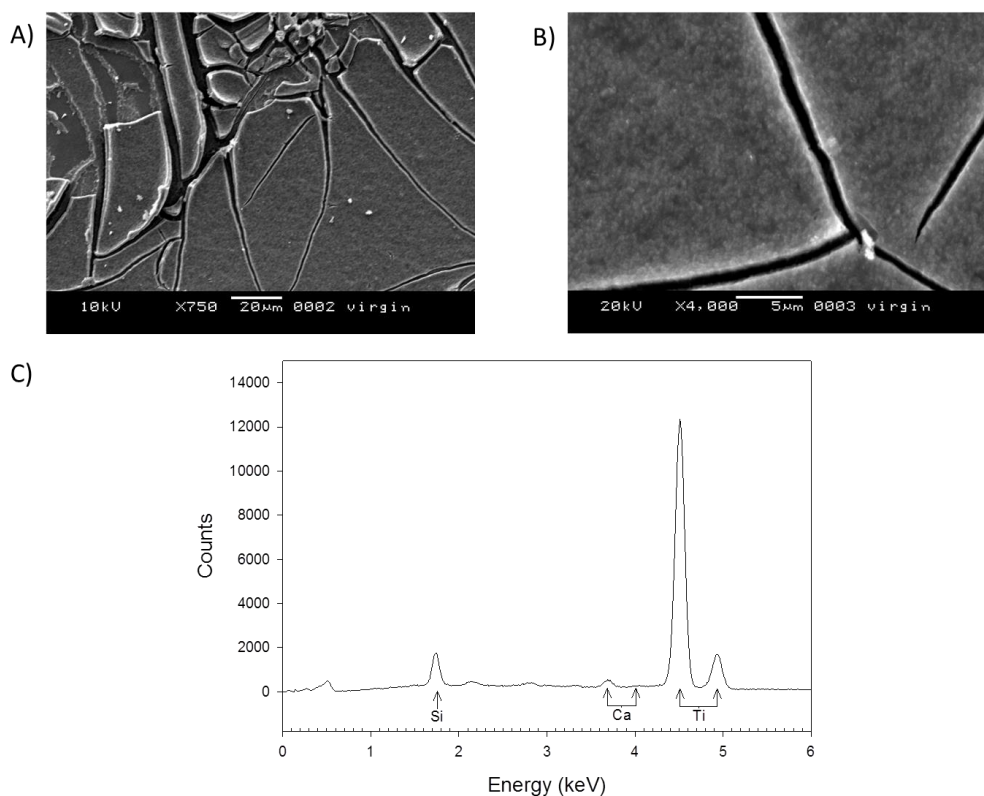


**Figure 3.1: SEM-EDS characterization of virgin catalyst films. A) 750× magnification SEM of catalyst surface. B) 4000× magnification SEM of catalyst surface. C) EDS spectrum of catalyst surface showing Ti and Si peaks.**

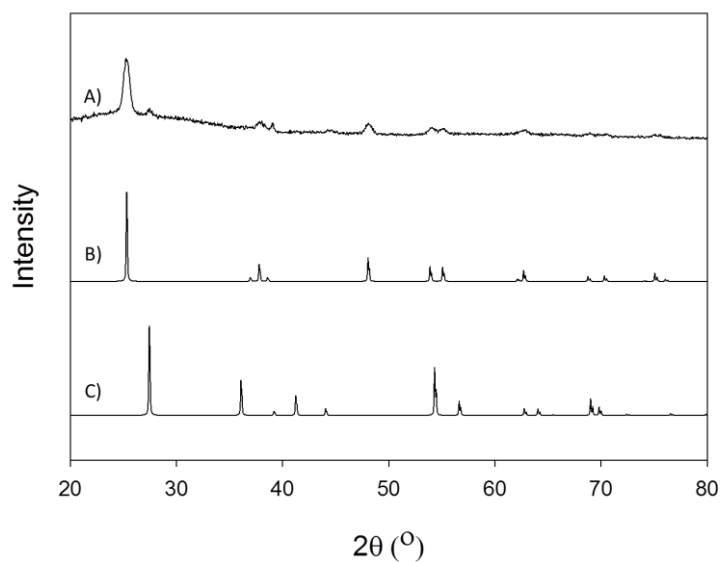


**Figure 3.2: XRD spectrum of A) virgin catalyst surface, with reference spectra of B) anatase<sup>42</sup> and C) rutile<sup>43</sup> phases of TiO<sub>2</sub>.**

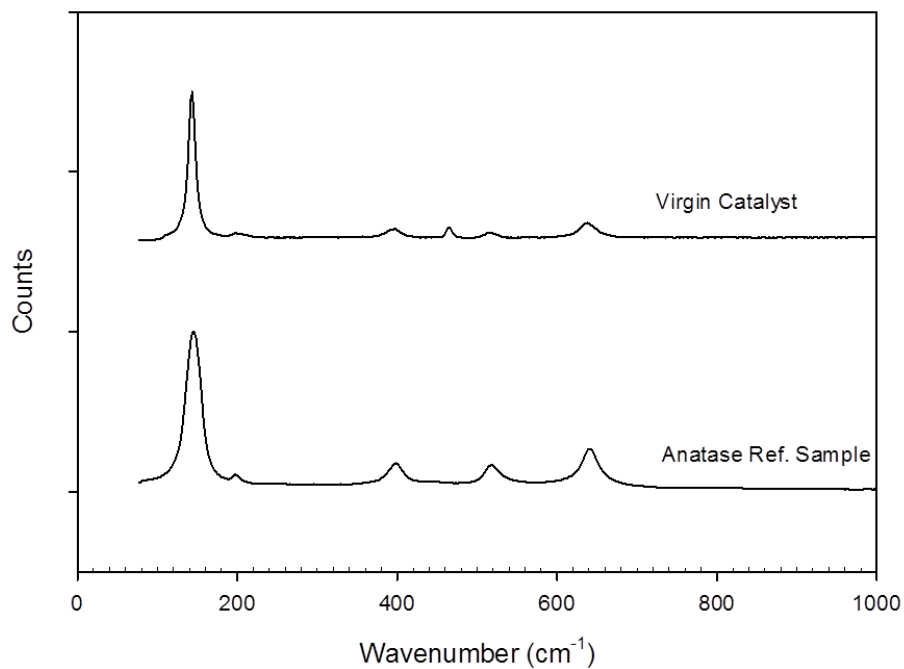


**Figure 3.3: Raman spectrum of virgin catalyst surface with reference spectrum of anatase<sup>44</sup>. Extra peak in virgin catalyst sample is attributed to glass substrate.**

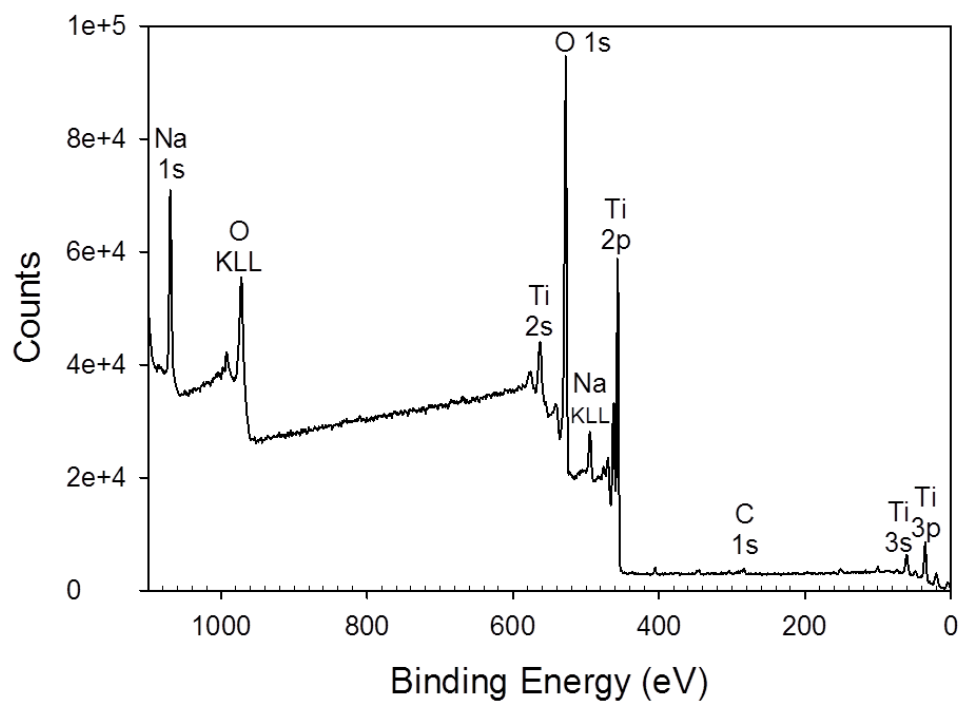


**Figure 3.4: XPS spectrum of virgin catalyst surface, showing strong Ti and O peaks. Na presence is attributed to impurities in the sol-gel preparation.**

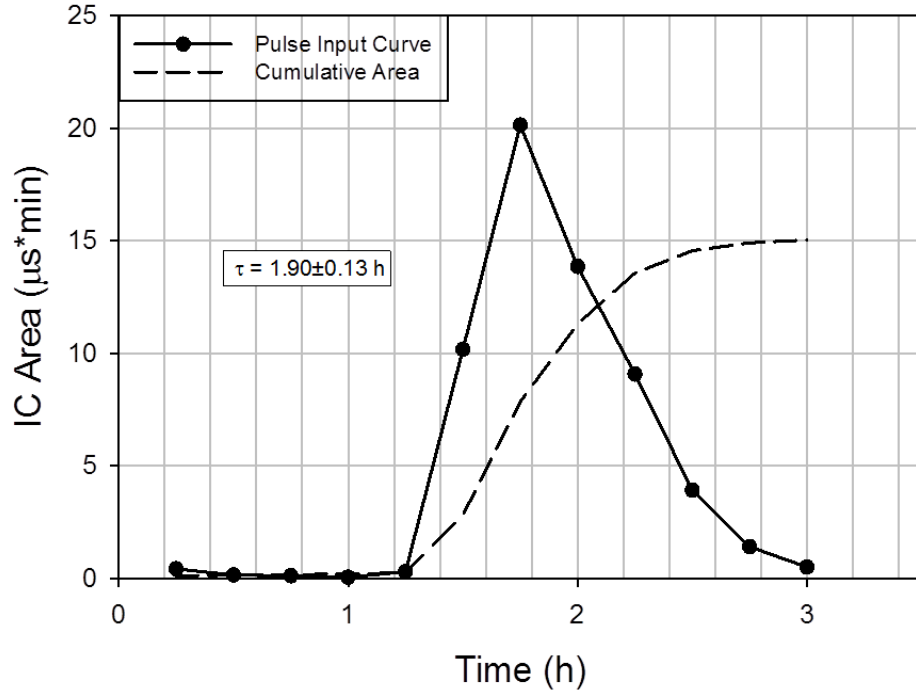


Figure 3.5: Results of perchlorate tracer test. Mean residence time ( $\tau$ ) was found to be  $1.90 \pm 0.13$  hours.

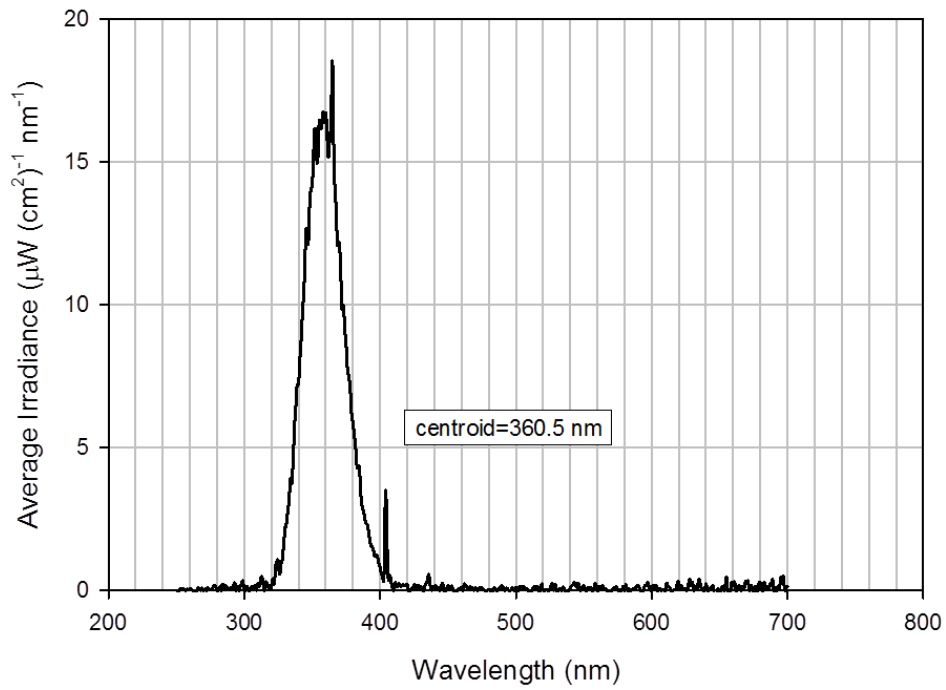
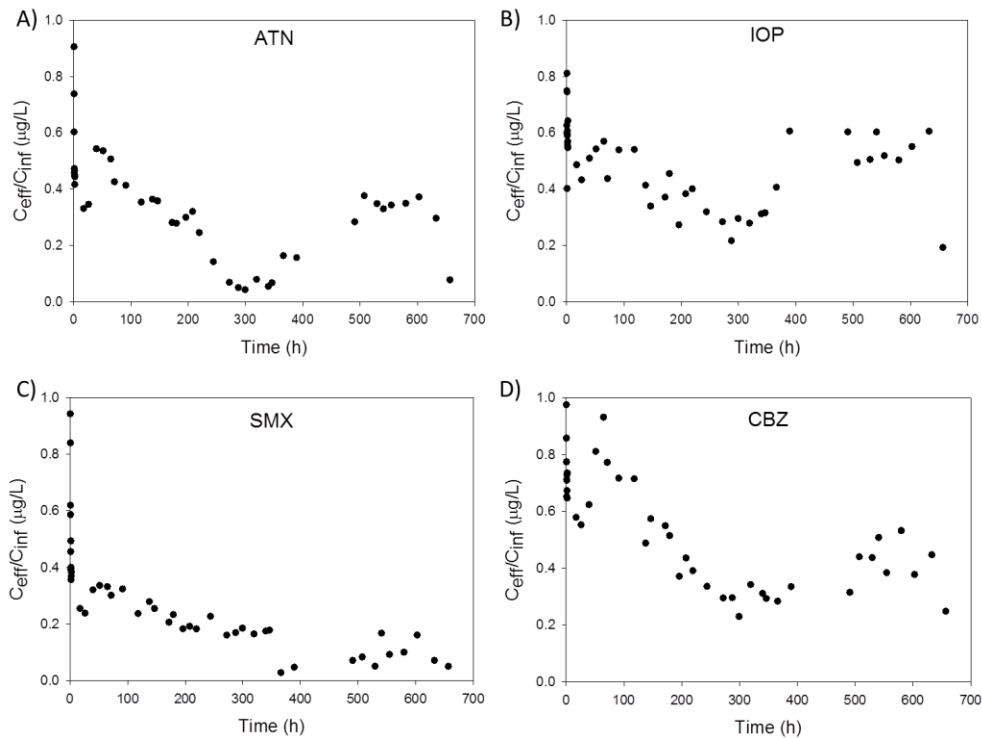
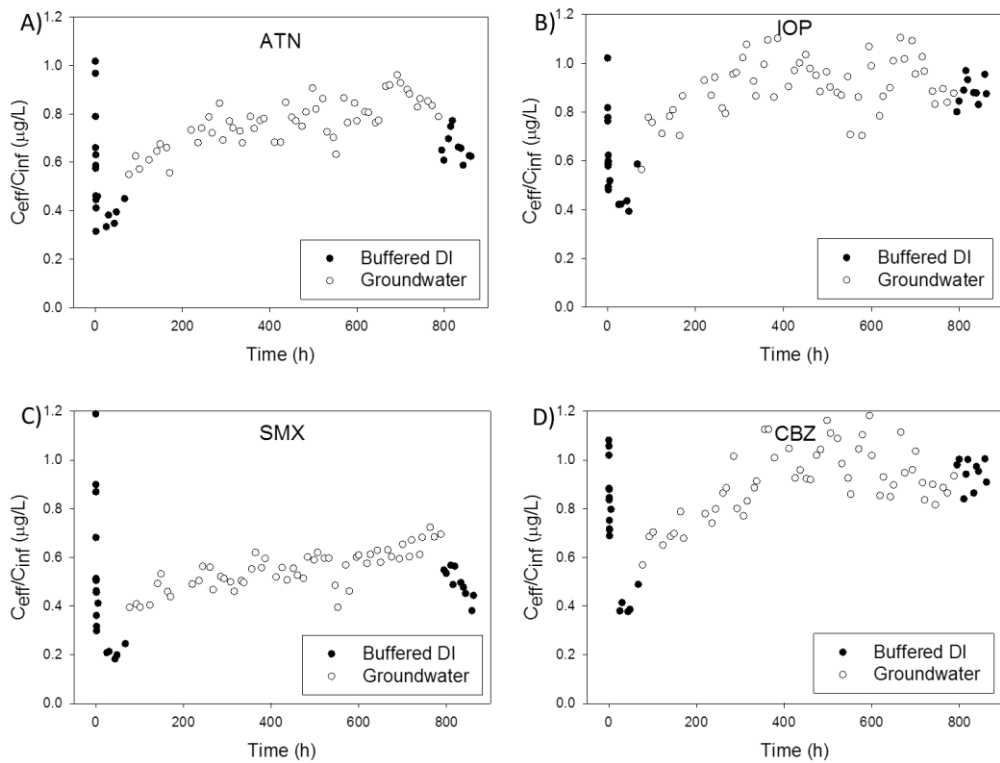


Figure 3.6: Average UV irradiance sampled from 30 points at the height of the catalysts (12 cm). Results show spectrum is centered at 360.5 nm, close to the manufacturer's specification of 365 nm.



**Figure 3.7: Results from the continuous buffered DI control experiment for A) ATN, B) IOP, C) SMX, D) CBZ.**



**Figure 3.8: Timecourse of the first 30 d of GW exposure in the reactor for A) ATN, B) IOP, C) SMX, and D) CBZ.**



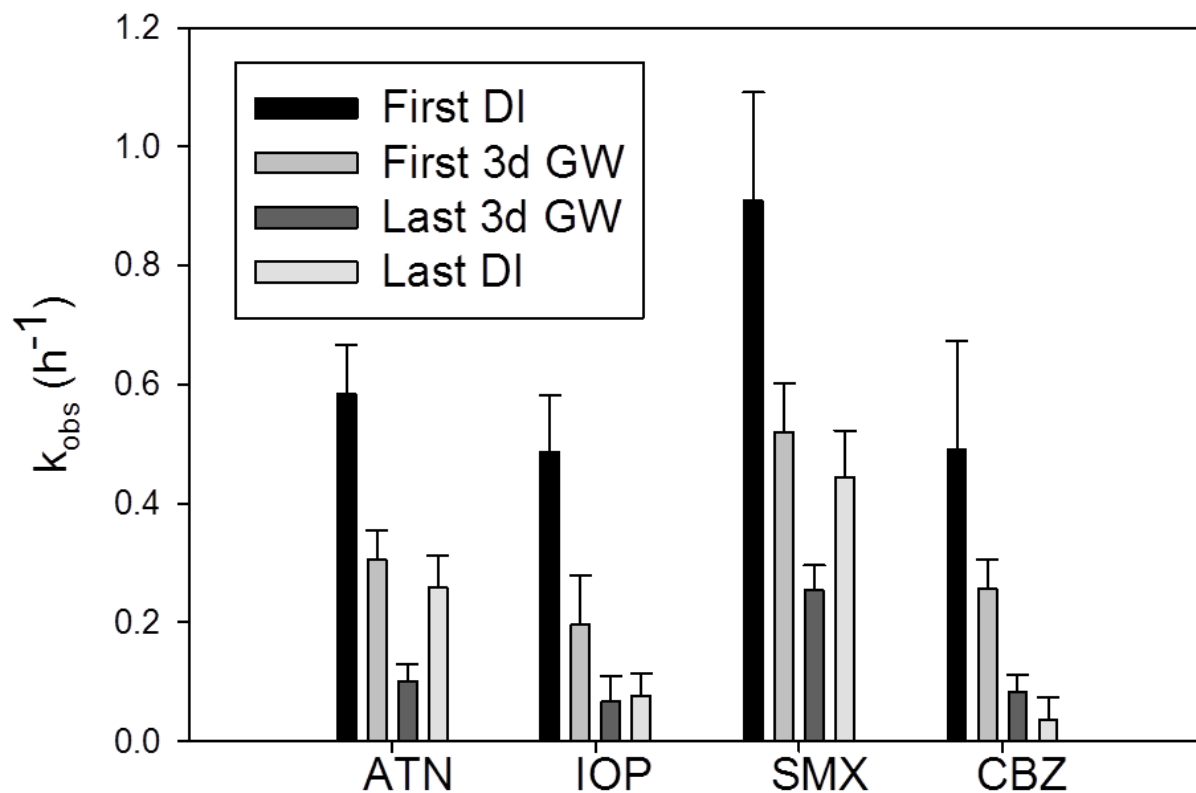


Figure 3.9: Pseudo-first order rate constants for both buffered DI exposures as well as the first and last three days of GW exposure. Error bars represent 1 standard deviation.

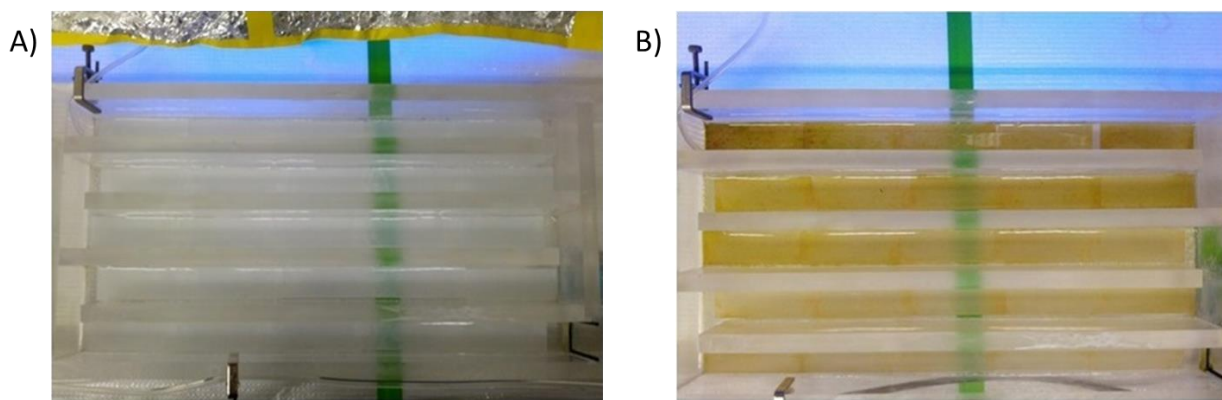
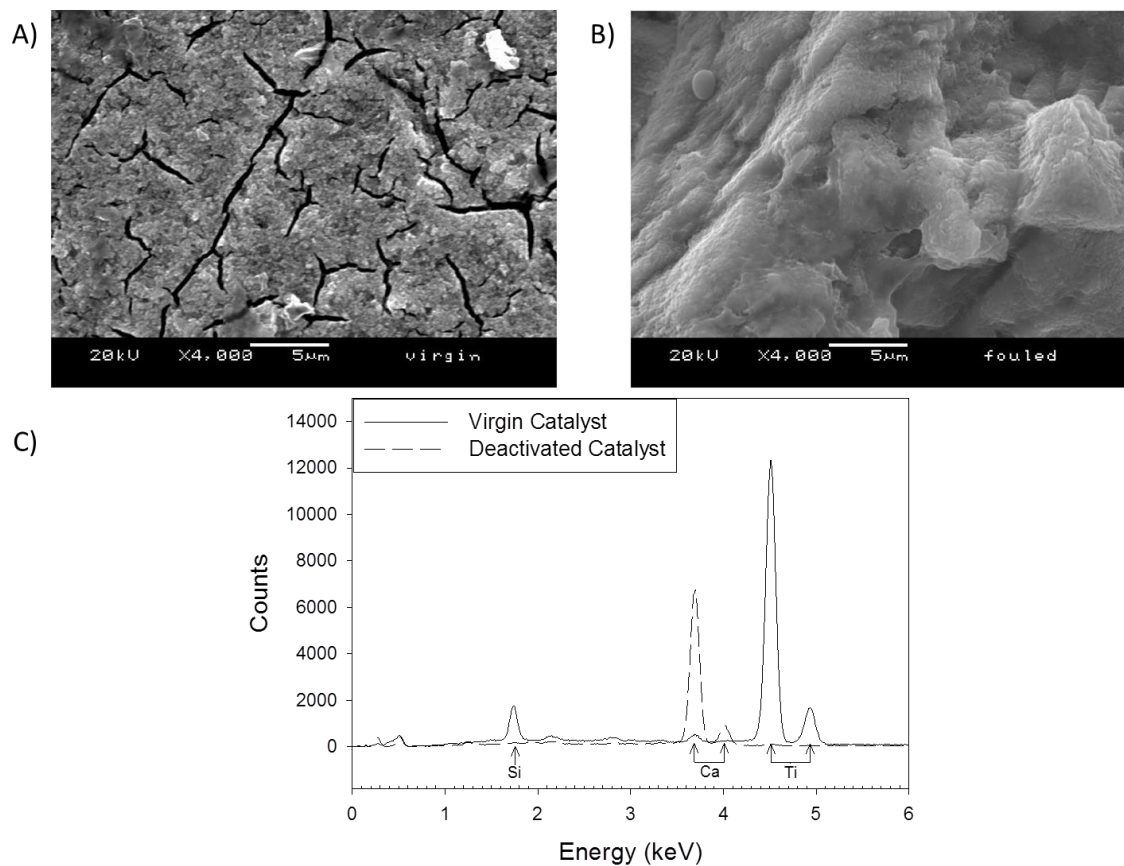
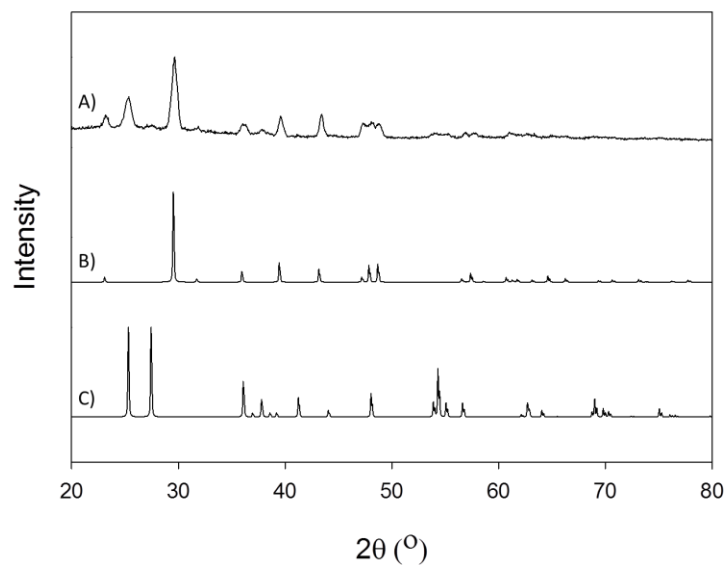


Figure 3.10: Development of discoloration in reactor on catalyst films after 30 d of GW exposure. A) Reactor before GW exposure. B) Reactor after 30 d.



**Figure 3.11: Comparison of SEM-EDS results for virgin and deactivated catalyst films at 4000x magnification. A) Virgin catalyst surface. B) Deactivated catalyst surface. C) EDS results showing Ca peaks on the deactivated catalyst and Ti and Si peaks on the virgin catalyst surface.**



**Figure 3.12: XRD spectra for deactivated catalyst (A) and a reference spectrum for calcite<sup>45</sup> (B), and a combined reference spectrum for anatase<sup>42</sup> and rutile<sup>43</sup> phases of  $\text{TiO}_2$  (C).**

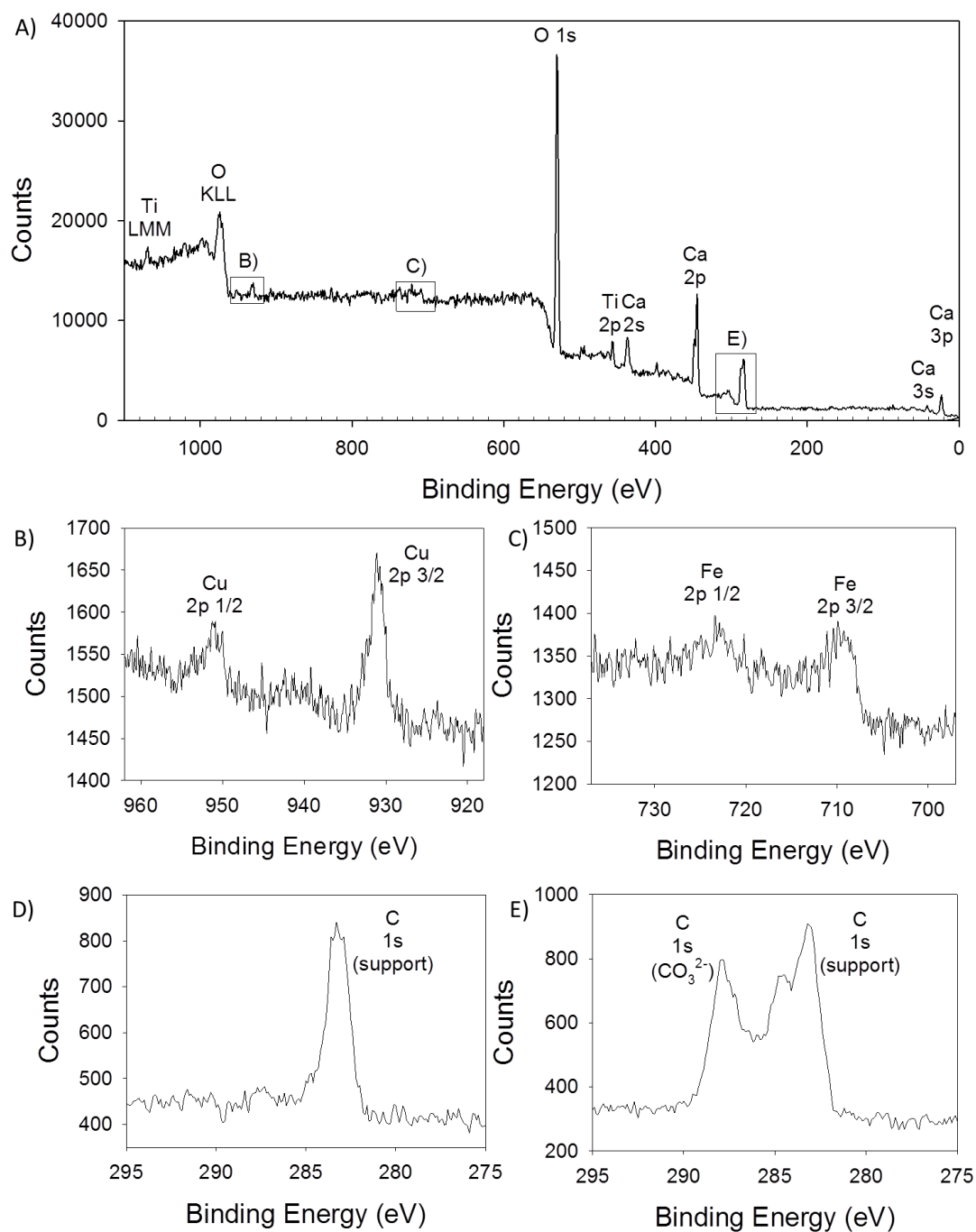


**Figure 3.13: XPS spectra of deactivated catalyst surface. A) Full scan indicating strong peaks from O, C, Ti, and Ca. B) Hi-res scan of Cu region showing peaks from Cu. C) Hi-res scan of Fe region showing Fe peaks. D) C peak from virgin slide for reference. E) C peaks from deactivated slide showing both adventitious carbon and carbonate present.**

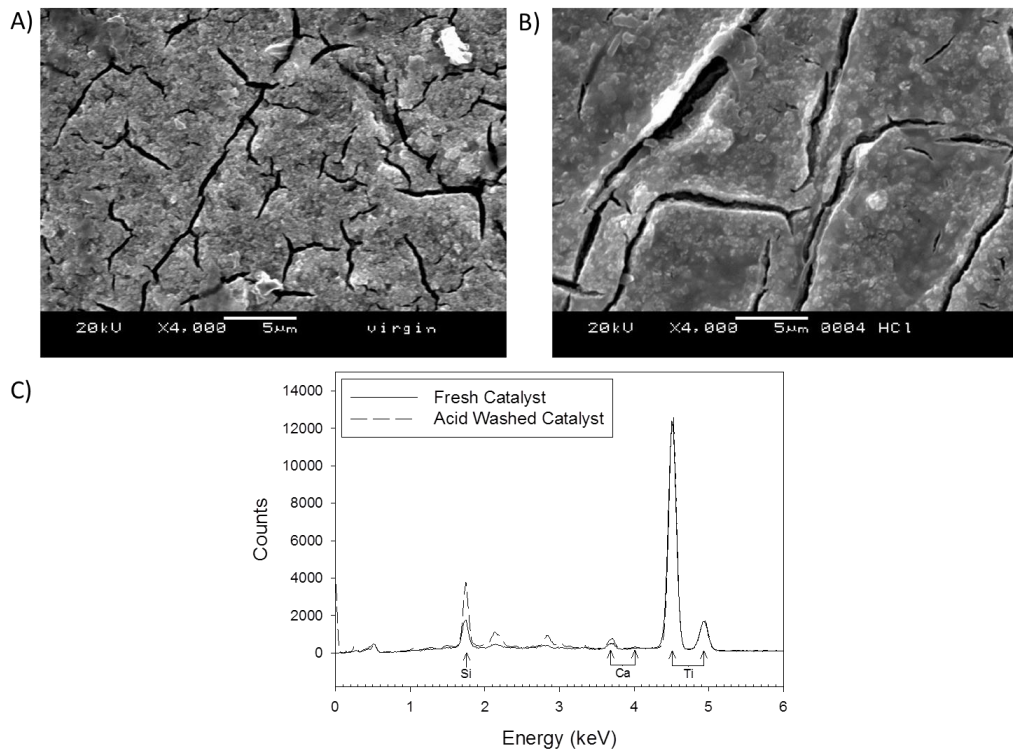


**Figure 3.14: Comparison of SEM-EDS results for virgin and hydrochloric acid-washed deactivated catalyst films from chemical treatment experiments at 4000x magnification. A) Virgin catalyst surface. B) Acid washed catalyst surface. C) EDS results showing Ca, Ti and Si peaks on the virgin catalyst surface.**

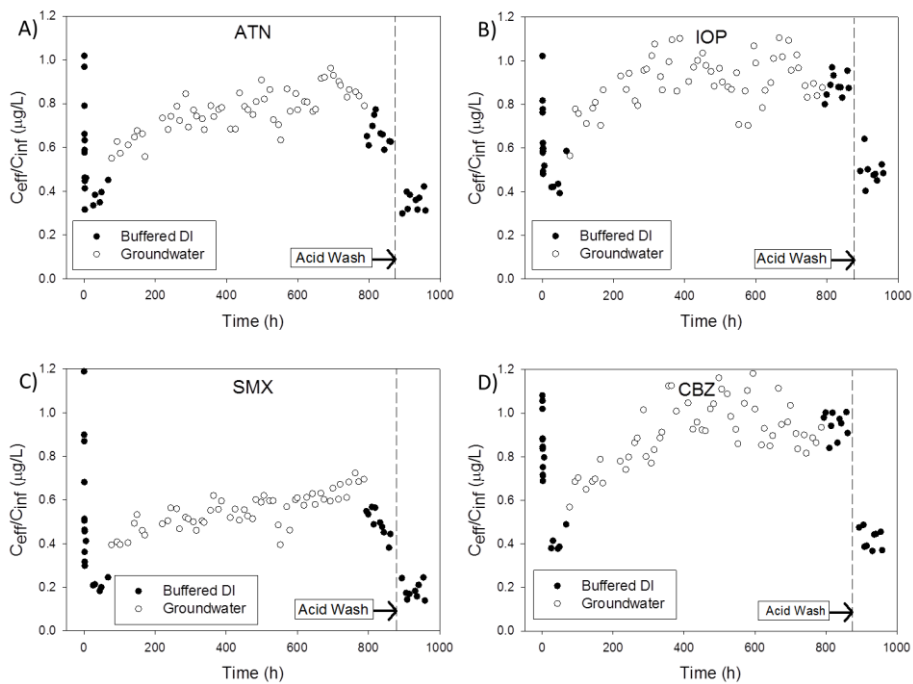


**Figure 3.15: Timecourse data including 24-hour acid wash following groundwater exposure for A) ATN, B) IOP, C) SMX, D) CBZ. Irreversible deactivation from the groundwater exposure is effectively removed by the acid wash.**

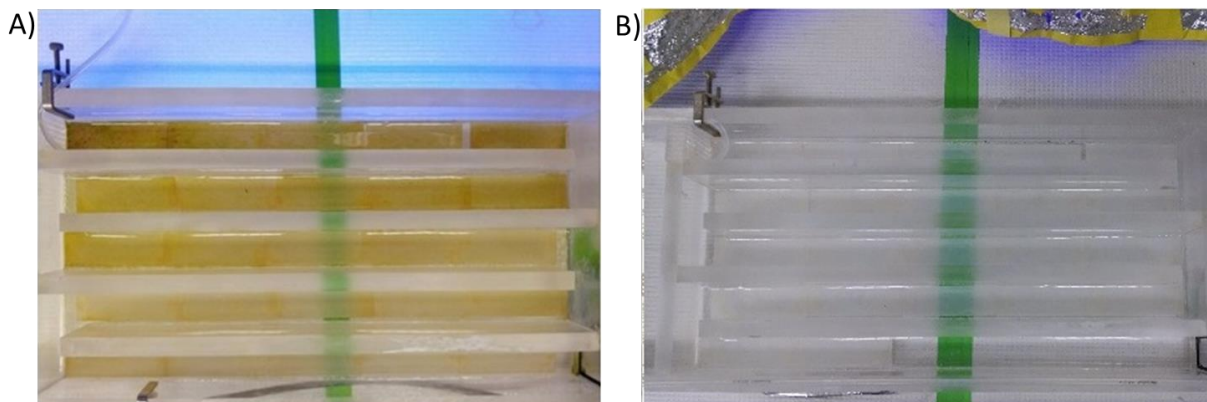


**Figure 3.16: Comparison of catalyst surfaces in reactor before (A) and after (B) acid washing. Catalysts returned to their initial white color after acid washing.**

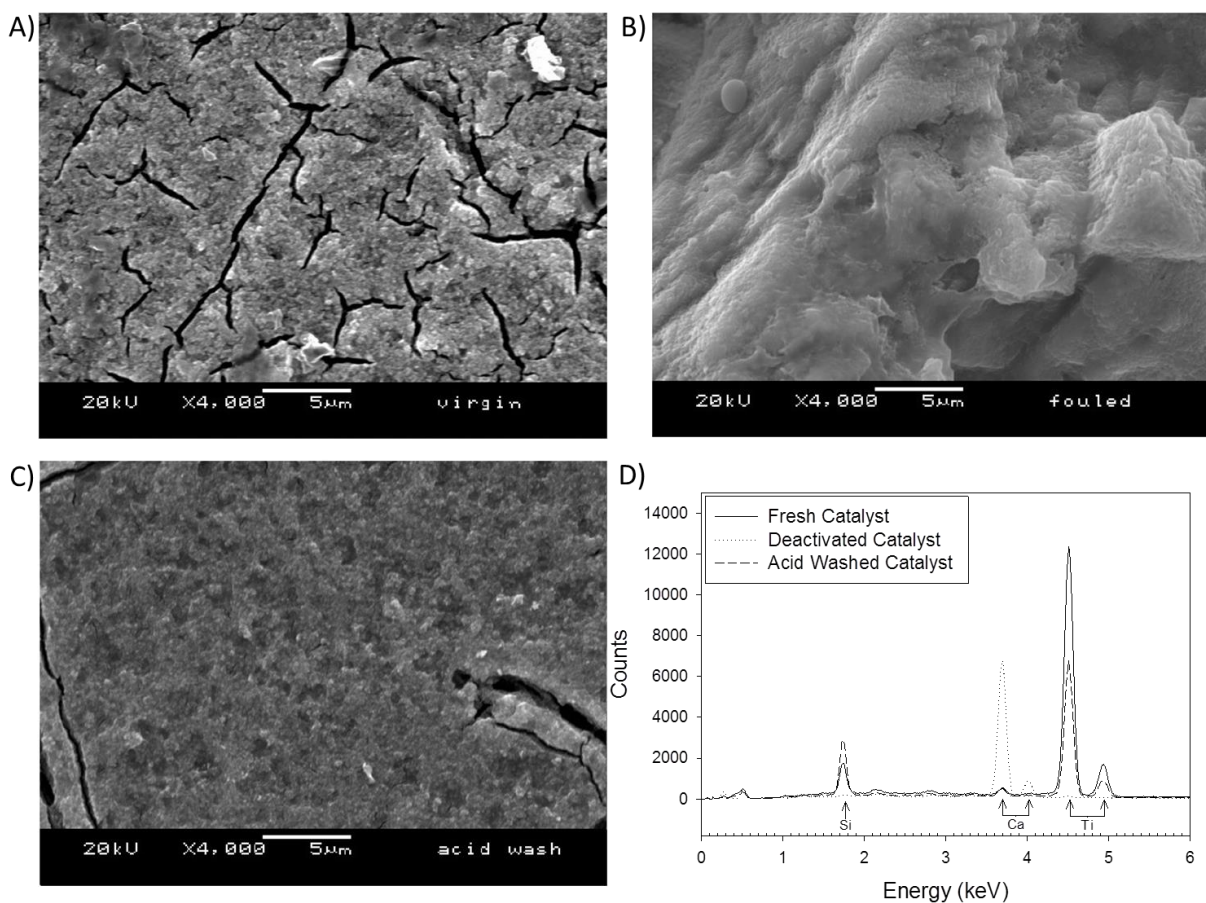


**Figure 3.17: SEM-EDS comparison of virgin, deactivated, and acid washed catalyst surfaces at 4000x magnification. After acid washing, catalysts had similar characteristics to that of the virgin catalyst surface. A) Virgin catalyst surface from Figure 3.11. B) Deactivated catalyst surface from Figure 3.11. C) Acid washed catalyst surface. D) EDS results showing significant reduction in Ca peak after acid washing.**

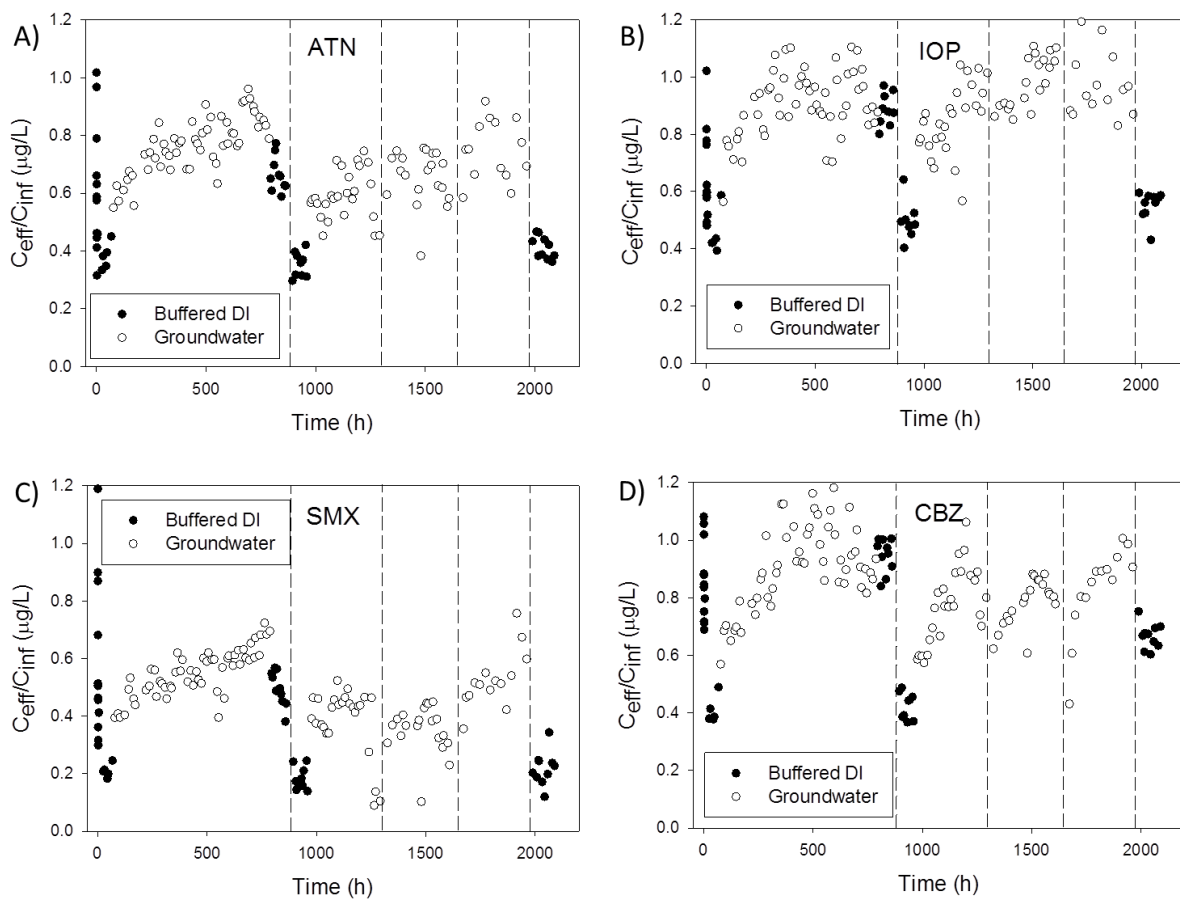


**Figure 3.18: Timecourse results of recurrent acid washing during groundwater exposure for A) ATN, B) IOP, C) SMX, and D) CBZ. Vertical dashed lines on the plots denote acid washings.**

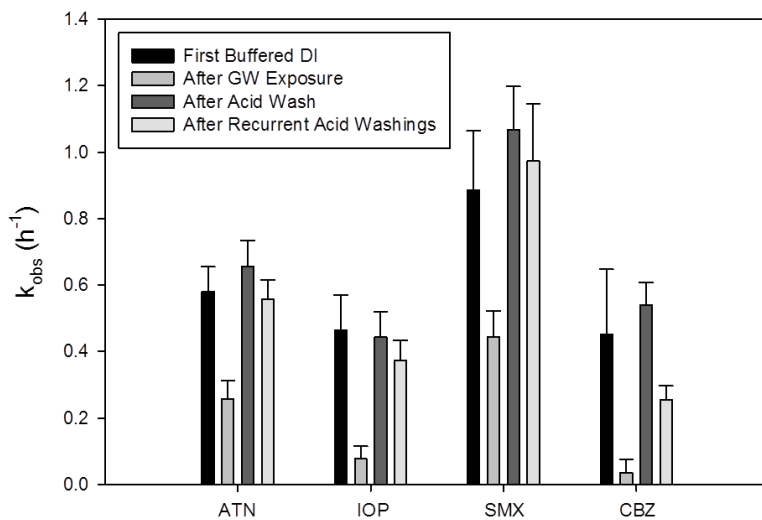


**Figure 3.19: Comparison of the pseudo-first order rate constants for the four three-day buffered DI exposures in the reactor. Some small loss in activity is observed; this may have been prevented by increasing the length of the acid wash or the acid concentration. Error bars represent one standard deviation.**

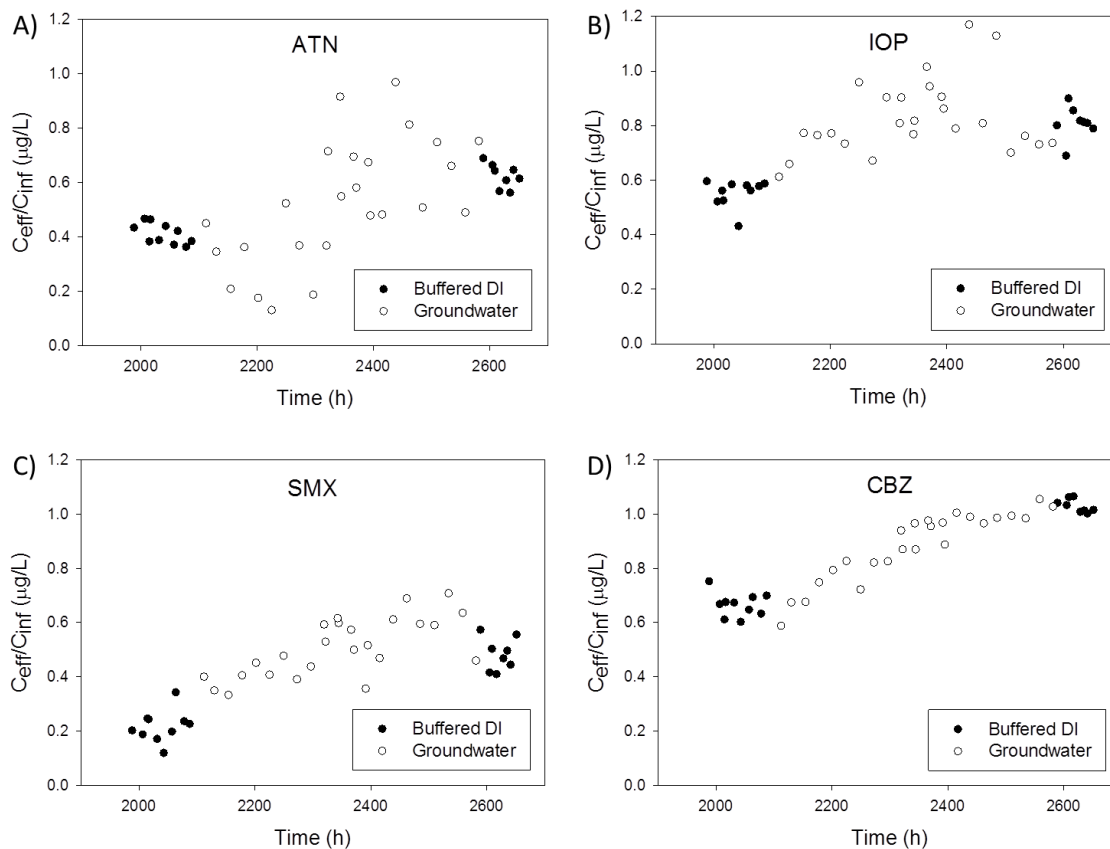


**Figure 3.20: Results from the softened groundwater experiment for A) ATN, B) IOP, C) SMX, and D) CBZ. Catalysts experienced similar deactivation as the unsoftened groundwater experiment.**

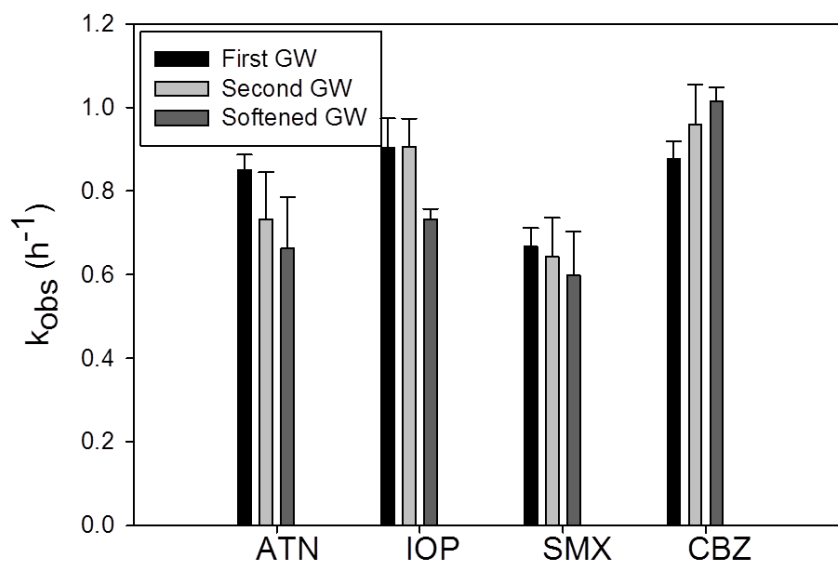


**Figure 3.21: Comparison of rate constants between the last three days of the first, second, and softened groundwater exposures in this study. The softened groundwater had a similar deactivating character to the unsoftened groundwater exposures. Error bars represent one standard deviation.**

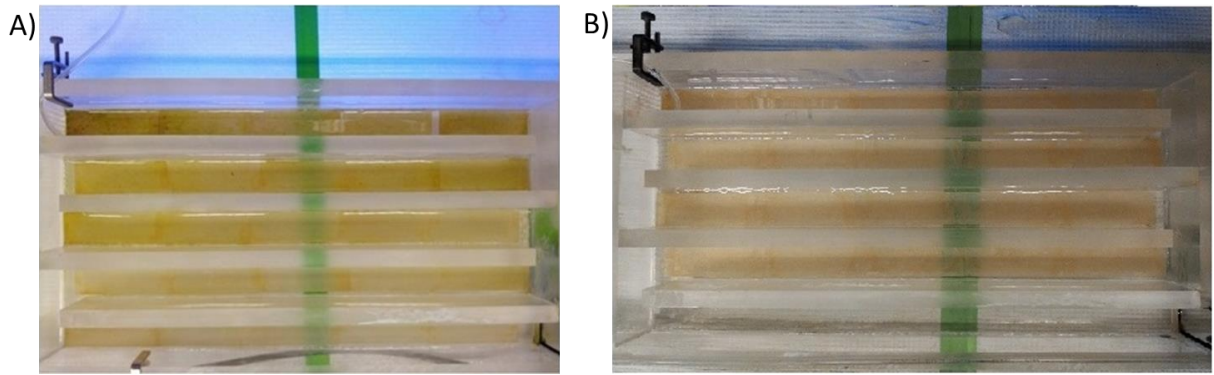


**Figure 3.22: Comparison of the reactor after the first groundwater exposure (A) and the softened groundwater experiment (B). The catalysts developed a similar brown discoloration.**

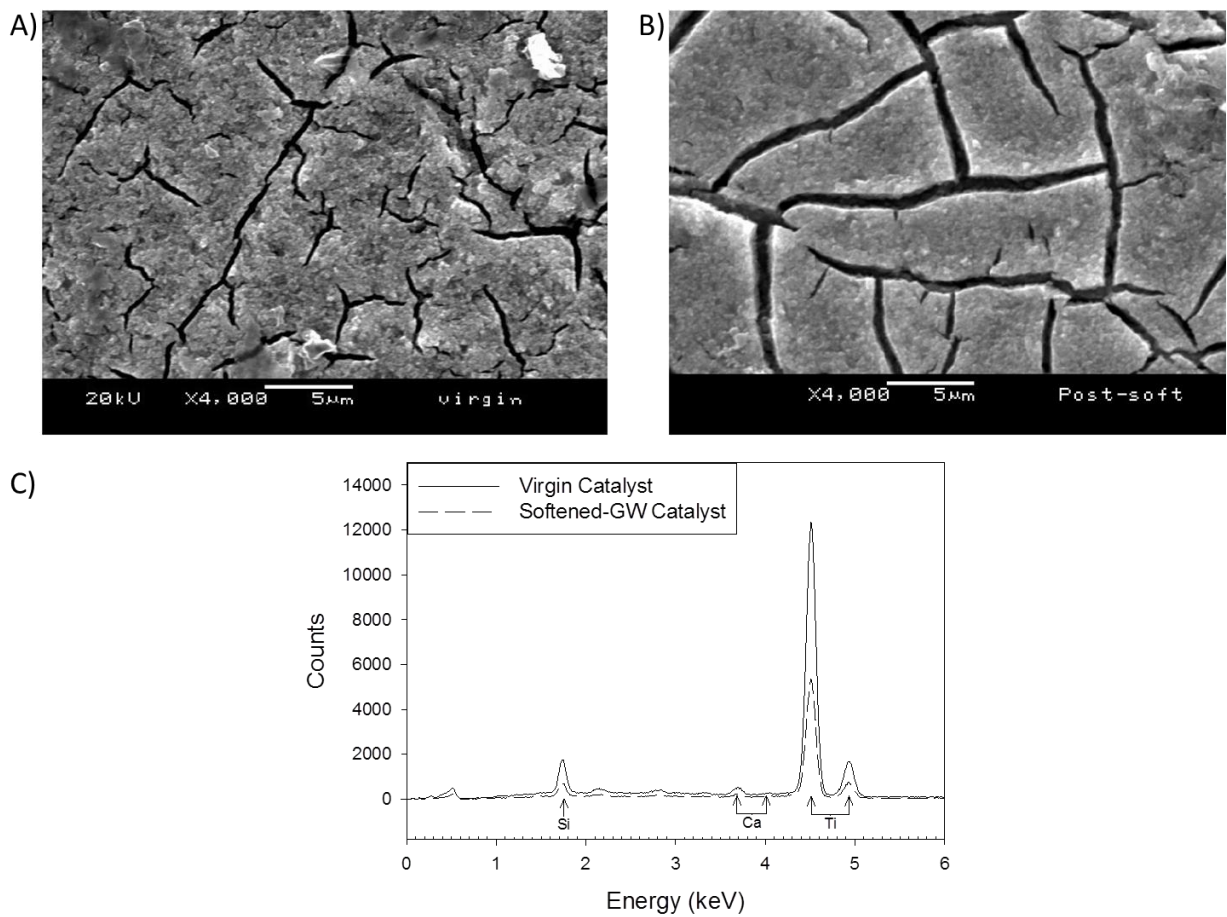


**Figure 3.23: SEM-EDS comparison between virgin catalyst surface and catalyst surface after deactivation from softened GW. A) SEM of virgin catalyst surface at 4000x magnification. B) SEM of softened-GW-deactivated catalyst surface at 4000x magnification. C) EDS comparison between both surfaces, showing mainly Ti and Si.**



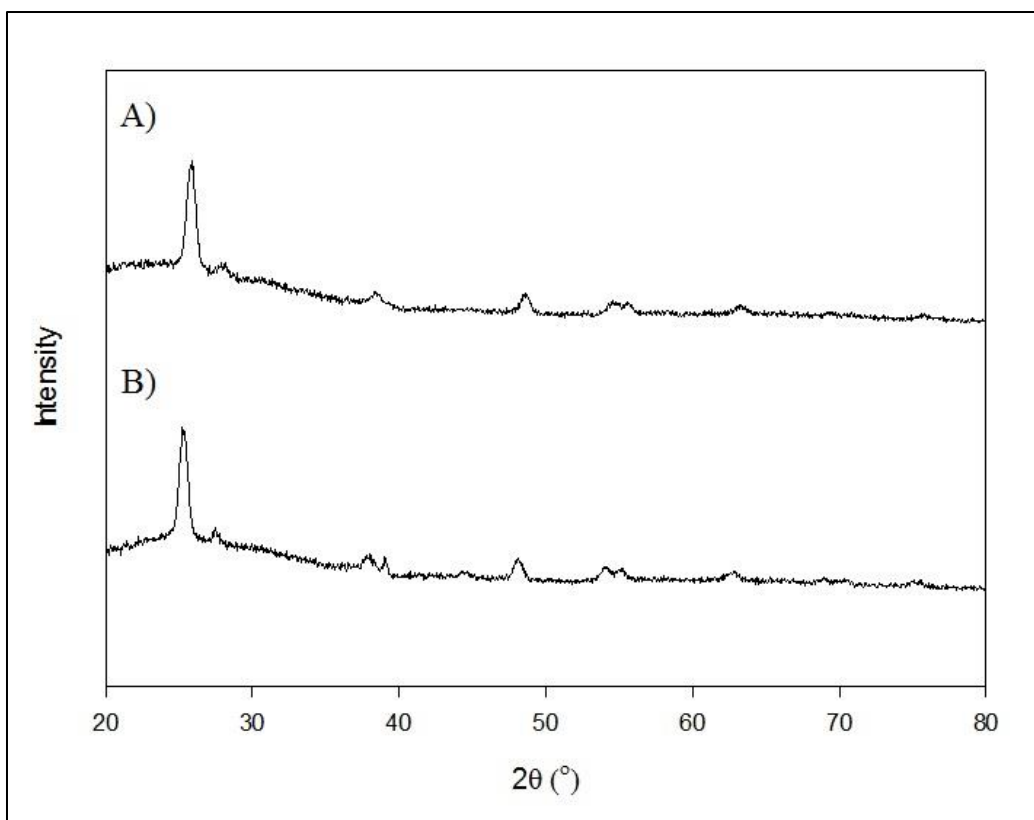


**Figure 3.24: Comparison between XRD spectra of A) catalyst surface after deactivation by softened groundwater and B) virgin catalyst surface. Results show nearly no difference between the two, indicating that the bulk TiO<sub>2</sub> signal is too strong relative to the trace deactivating material.**

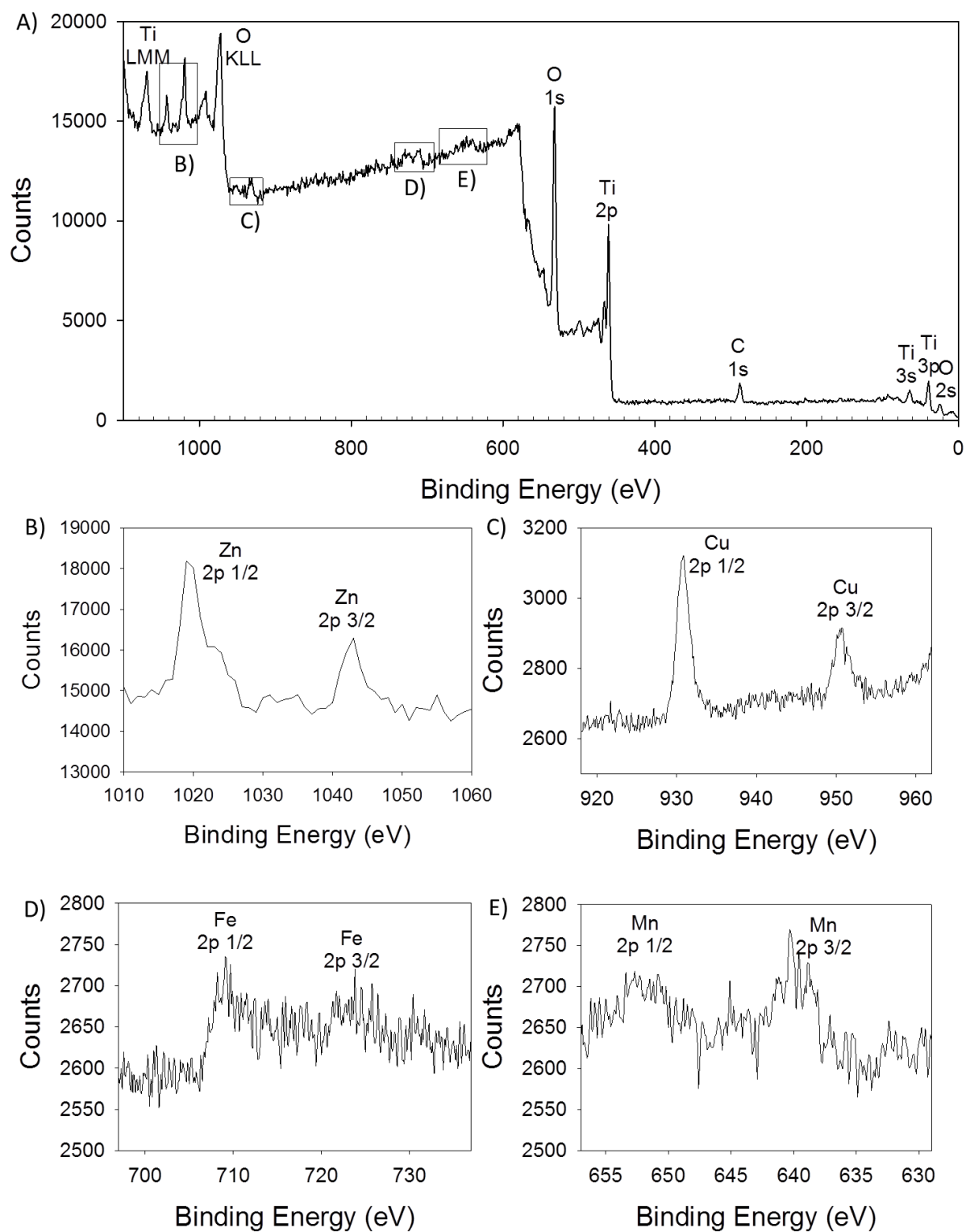


**Figure 3.25: XPS spectra of catalyst deactivated by softened GW. A) Full spectrum. B) Hi-res scan of Zn spectrum. C) Hi-res scan of Cu spectrum. D) Hi-res scan of Fe spectrum. E) Hi-res scan of Mn spectrum.**

Characteristic	Buffered DI	Real Groundwater Matrix
pH	8.41	8.46±0.02
Alkalinity (mg/L as CaCO <sub>3</sub> )	209.1	217.7±8.0
DOC (mg/L)	0	1.52±0.01
Major Dissolved Constituents	NaHCO <sub>3</sub> (4.306 mM)	HCO <sub>3</sub> <sup>-</sup> (4.3 mM) (estimated from alkalinity); Cl <sup>-</sup> (24.7±5.5 μM); NO <sub>3</sub> <sup>-</sup> (16.2±10.2 μM); SO <sub>4</sub> <sup>2-</sup> (12.0±2.0 μM); F <sup>-</sup> (3.4±1.1 μM); PO <sub>4</sub> <sup>3-</sup> (2.9±0.1 μM); Br <sup>-</sup> (1.8±0.1 μM) Ca (34.08±0.86 ppm); Mg (23.94±1.92 ppm); Na (22.64±2.63 ppm); Be (13.57±7.0 ppm); Si (6.73±1.00 ppm); Li (4.29±3.78 ppm); K (1.03±0.08 ppm); Cu (204±260 ppb); Ba (88±18 ppb); Zn (20±17 ppb); Mn (2.96±2.09 ppb)

**Table 3.1: Major characteristics of buffered DI and real groundwater matrices. Samples including standard deviation values were averaged over 3 GW samples taken 2 weeks apart from each other during the 30d initial GW study and the subsequent recurring acid treatment study. Note that DOC values are significantly higher (~10<sup>3</sup>) than target PPCP concentrations.**

Characteristic	Influent GW	Effluent GW
pH	8.46±0.02	8.51±0.02
Alkalinity (mg/L as CaCO <sub>3</sub> )	217.7±8.0	240.0±6.6
DOC (mg/L)	1.52±0.01	1.54±0.13
Major Dissolved Constituents	HCO <sub>3</sub> <sup>-</sup> (4.3 mM) (estimated from alkalinity); Cl <sup>-</sup> (24.7±5.5 μM); NO <sub>3</sub> <sup>-</sup> (16.2±10.2 μM); SO <sub>4</sub> <sup>2-</sup> (12.0±2.0 μM); F <sup>-</sup> (3.4±1.1 μM); PO <sub>4</sub> <sup>3-</sup> (2.9±0.1 μM); Br <sup>-</sup> (1.8±0.1 μM) Ca (34.08±0.86 ppm); Mg (23.94±1.92 ppm); Na (22.64±2.63 ppm); Be (13.57±7.0 ppm); Si (6.73±1.00 ppm); Li (4.29±3.78 ppm); K (1.03±0.08 ppm); Cu (204±260 ppb); Ba (88±18 ppb); Zn (20±17 ppb); Mn (2.96±2.09 ppb)	HCO <sub>3</sub> <sup>-</sup> (4.8 mM) (estimated from alkalinity); Cl <sup>-</sup> (21.3±2.0 μM); NO <sub>3</sub> <sup>-</sup> (7.0±1.0 μM); SO <sub>4</sub> <sup>2-</sup> (13.4±0.5 μM); F <sup>-</sup> (4.1±0.6 μM); PO <sub>4</sub> <sup>3-</sup> (2.9±0.1 μM); Br <sup>-</sup> (1.8±0.1 μM) Ca (34.07±1.12 ppm); Mg (26.04±1.64 ppm); Na (25.13±2.64 ppm); Be (14.74±9.13 ppm); Si (7.20±1.32 ppm); Li (5.25±5.01 ppm); K (1.26±0.16 ppm); Cu (7±1 ppb); Ba (75±3 ppb); Zn (10±0 ppb); Mn (2.79±2.18 ppb)

**Table 3.2: Comparison of characteristics of GW matrix in the influent reservoir and collected effluent. Data were averaged from 3 influent and 3 effluent samples taken ~2 weeks apart from each other during the initial 30d GW treatment and subsequent recurrent acid washing treatment.**

Treatment Chemical	Group	Concentration
Ascorbic Acid	Acid/reductant	10 mM
Hydrochloric Acid	Acid	100 mM
Sodium Hydroxide	Base	100 mM
Sodium Hypochlorite	Oxidant	10 mM
EDTA (Tetrasodium salt)	Chelator	10 mM
Sodium Percarbonate	Oxidant	10 mM
Anionic Detergent	Surfactant	25% saturated

**Table 3.3: List of chemicals used in catalyst treatment experiments. Note that the HCl concentration used here is 100 mM and later acid treatments in the reactor used 10 mM HCl.**

Element	Weight % of Total	Element	Weight % of Total
Ca	7.61	Al	0.16
Na	4.8	Be	0.14
Mg	4.7	Sr	0.082
Si	1.99	Mn	0.077
Cu	0.86	Sn	0.067
Li	0.7	Ti	0.038
Fe	0.65	P	0.03
K	0.59	Br	0.021
Zn	0.34	Ba	0.012

**Table 3.4: ICP-MS analysis of evaporated acid wash effluent. Elements listed were observed at greater than 0.01% of the total solids. The remaining ~80% of solids not measured by ICP-MS is assumed to be anionic species ( $\text{CO}_3^{2-}$ ,  $\text{SO}_4^{2-}$ ,  $\text{NO}_3^-$ ,  $\text{PO}_4^{3-}$ ,  $\text{Cl}^-$ ,  $\text{Br}^-$ , and  $\text{F}^-$  are all present) and trace species.**

Characteristic	Before Softening	After Softening
<b>pH</b>	8.27	8.69
<b>Alkalinity (mg/L as CaCO<sub>3</sub>)</b>	225.0	220.0
<b>DOC (mg/L)</b>	1.416	1.408
<b>Major Dissolved Constituents</b>	HCO <sub>3</sub> <sup>-</sup> (4.5 mM) (estimated from alkalinity); Cl <sup>-</sup> (23.5 μM); NO <sub>3</sub> <sup>-</sup> (4.15 μM); SO <sub>4</sub> <sup>2-</sup> (11.4 μM); F <sup>-</sup> (3.2 μM); PO <sub>4</sub> <sup>3-</sup> (2.9 μM); Br <sup>-</sup> (1.9 μM) Ca (17.3 ppm); Mg (23.5 ppm); Na (20.8 ppm); Be (5.7 ppm); Si (6.3 ppm); Li (1.2 ppm); K (1.0 ppm); Cu (11 ppb); Cr (6 ppb); Zn (2 ppb); Mn (3 ppb)	HCO <sub>3</sub> <sup>-</sup> (4.5 mM) (estimated from alkalinity); Cl <sup>-</sup> (22.4 μM); NO <sub>3</sub> <sup>-</sup> (5.66 μM); SO <sub>4</sub> <sup>2-</sup> (11.3 μM); F <sup>-</sup> (2.2 μM); PO <sub>4</sub> <sup>3-</sup> (2.9 μM); Br <sup>-</sup> (1.8 μM) Ca (0.56 ppm); Mg (0.24 ppm); Na (77.4 ppm); Be (4.6 ppm); Si (5.9 ppm); Li (1.2 ppm); K (0.05 ppm); Cu (1 ppb); Cr (5 ppb); Zn (1 ppb); Mn (0)

**Table 3.5: ICP-MS analyses of groundwater matrix before and after passing through a sodium ion-exchange softening resin.**

## 4. CONCLUSIONS

In this contribution, a novel flow-through reactor for immobilized-TiO<sub>2</sub> UV-photocatalysis of PPCPs in real water matrices was studied. In particular, the effects of long-term (1 month) exposure to groundwater containing µg/L concentrations of target PPCP compounds were assessed. Results show that long-term exposure to groundwater matrices inhibits TiO<sub>2</sub> catalyst activity, potentially both from physical blocking of UV radiation and active catalyst sites from mineral precipitation (e.g., calcite), and from antagonistic effects on TiO<sub>2</sub> photoactivity from adsorbed trace metal species (e.g., Fe, Zn, Cu, and Mn). The loss of PPCP removal from catalyst inactivation varies by compound, and PPCP compounds with aniline groups or other moieties that are reactive with carbonate radicals still undergo some degradation even after other target compounds are no longer degraded. Catalyst inhibition can be reversed by using chemical treatment (e.g. rinsing films with hydrochloric acid) to dissolve/desorb catalyst-deactivating metal species; results show that the catalyst surface retains its photoactivity after several acid rinsing treatments. Similarly to membrane processes, recurrent chemical treatment can be employed in the reactor to remove deactivating material. Pretreatment of influent groundwater matrices with cation-exchange softening resins to prevent precipitation of calcite still results in catalyst deactivation over a similar time frame; this lends support to the idea that trace metals deposited on the catalyst surface interfere with TiO<sub>2</sub> photoactivity. Further work is needed to investigate other methods of pretreatment of the groundwater matrix to prevent catalyst deactivation. pH modification could be employed to prevent metal precipitation and inhibit metal adsorption on the catalyst surface; also, introducing a more frequent chemical treatment step to the reactor (e.g., every 24 h as opposed to the 2 wk period used in this study) could potentially extend catalyst viability.

## 5. REFERENCES

- (1) Daughton, C. G.; Ternes, T. A. *Environ. Health Perspect.* **1999**, *107 Suppl 6*, 907–938.
- (2) Boyd, G. R.; Reemtsma, H.; Grimm, D. A.; Mitra, S. *Sci. Total Environ.* **2003**, *311*, 135–149.
- (3) Ternes, T. A. *Water Res.* **1998**, *32*, 3245–3260.
- (4) Jobling, S.; Nolan, M.; Tyler, C. R.; Brighty, G.; Sumpter, J. P. *Environ. Sci. Technol.* **1998**, *32*, 2498–2506.
- (5) Falconer, I. R.; Chapman, H. F.; Moore, M. R.; Ranmuthugala, G. *Environ. Toxicol.* **2006**, *21*, 181–191.
- (6) Drewes, J. E.; Heberer, T.; Rauch, T.; Reddersen, K. *Ground Water Monit. Remediat.* **2003**, *23*, 64–72.
- (7) Kinney, C. A.; Furlong, E. T.; Werner, S. L.; Cahill, J. D. *Environ. Toxicol. Chem.* **2006**, *25*, 317–326.
- (8) Barnes, K. K.; Kolpin, D. W.; Furlong, E. T.; Zaugg, S. D.; Meyer, M. T.; Barber, L. B. *Sci. Total Environ.* **2008**, *402*, 192–200.
- (9) Kuroda, K.; Murakami, M.; Oguma, K.; Muramatsu, Y.; Takada, H.; Takizawa, S. *Environ. Sci. Technol.* **2012**, *46*, 1455–1464.
- (10) Loos, R.; Locoro, G.; Comero, S.; Contini, S.; Schwesig, D.; Werres, F.; Balsaa, P.; Gans, O.; Weiss, S.; Blaha, L.; Bolchi, M.; Gawlik, B. M. *Water Res.* **2010**, *44*, 4115–4126.
- (11) Heberer, T.; Mechlinski, A.; Fanck, B.; Knappe, A.; Massmann, G.; Pekdeger, A.; Fritz, B. *Ground Water Monit. Remediat.* **2004**, *24*, 70–77.
- (12) Karnjanapiboonwong, A.; Suski, J. G.; Shah, A. A.; Cai, Q.; Morse, A. N.; Anderson, T. A. *Water, Air, Soil Pollut.* **2011**, *216*, 257–273.
- (13) Oulton, R. L.; Kohn, T.; Cwiertny, D. M. *J. Environ. Monit.* **2010**, *12*, 1956–1978.
- (14) Miège, C.; Choubert, J. M.; Ribeiro, L.; Eusèbe, M.; Coquery, M. *Environ. Pollut.* **2009**, *157*, 1721–1726.
- (15) Andreozzi, R.; Caprio, V.; Insola, A.; Marotta, R. *Catal. Today* **1999**, *53*, 51–59.
- (16) Ji, Y.; Zhou, L.; Ferronato, C.; Yang, X.; Salvador, A.; Zeng, C.; Chovelon, J.-M. *J. Photochem. Photobiol. Chem.* **2013**, *254*, 35–44.
- (17) Paul, T.; Dodd, M. C.; Strathmann, T. J. *Water Res.* **2010**, *44*, 3121–3132.
- (18) Paul, T.; Miller, P. L.; Strathmann, T. J. *Environ. Sci. Technol.* **2007**, *41*, 4720–4727.
- (19) Hu, L.; Flanders, P. M.; Miller, P. L.; Strathmann, T. J. *Water Res.* **2007**, *41*, 2612–2626.
- (20) Gaya, U. I.; Abdullah, A. H. *J. Photochem. Photobiol. C Photochem. Rev.* **2008**, *9*, 1–12.
- (21) Linsebigler, A. L.; Lu, G.; Yates, J. T. *Chem. Rev.* **1995**, *95*, 735–758.
- (22) Fujishima, A.; Zhang, X. *Comptes Rendus Chim.* **2006**, *9*, 750–760.
- (23) Daghrir, R.; Drogui, P.; Robert, D. *Ind. Eng. Chem. Res.* **2013**, *52*, 3581–3599.
- (24) Reyes, C.; Fernández, J.; Freer, J.; Mondaca, M. A.; Zaror, C.; Malato, S.; Mansilla, H. D. *J. Photochem. Photobiol. Chem.* **2006**, *184*, 141–146.
- (25) Sunada, K.; Kikuchi, Y.; Hashimoto, K.; Fujishima, A. *Environ. Sci. Technol.* **1998**, *32*, 726–728.

- (26) Doll, T. E.; Frimmel, F. H. *Water Res.* **2005**, *39*, 403–411.
- (27) Klammerth, N.; Miranda, N.; Malato, S.; Agüera, A.; Fernández-Alba, A. R.; Maldonado, M. I.; Coronado, J. M. *Catal. Today* **2009**, *144*, 124–130.
- (28) Calza, P.; Sakkas, V. A.; Medana, C.; Baiocchi, C.; Dimou, A.; Pelizzetti, E.; Albanis, T. *Appl. Catal. B Environ.* **2006**, *67*, 197–205.
- (29) N A Laoufi, S. H. *Chem. Eng. Trans.* **2013**, *32*, 1951–1956.
- (30) Carbonaro, S.; Sugihara, M. N.; Strathmann, T. J. *Appl. Catal. B Environ.* **2013**, *129*, 1–12.
- (31) Ohno, T.; Sarukawa, K.; Tokieda, K.; Matsumura, M. *J. Catal.* **2001**, *203*, 82–86.
- (32) *Standard Methods for the Examination of Water and Wastewater*; American Public Health Association., 1915.
- (33) Haynes, W. M. *CRC Handbook of Chemistry and Physics, 95th Edition*; Taylor & Francis, 2014.
- (34) Hapeshi, E.; Achilleos, A.; Vasquez, M. I.; Michael, C.; Xekoukoulotakis, N. P.; Mantzavinos, D.; Kassinos, D. *Water Res.* **2010**, *44*, 1737–1746.
- (35) Larson, R. A.; Zepp, R. G. *Environ. Toxicol. Chem.* **1988**, *7*, 265–274.
- (36) Jasper, J. T.; Sedlak, D. L. *Environ. Sci. Technol.* **2013**, *47*, 10781–10790.
- (37) Ni, M.; Ratner, B. D. *Surf. Interface Anal.* **2008**, *40*, 1356–1361.
- (38) Friedman, G. M. *J. Sediment. Res.* **1959**, *29*.
- (39) Di Paola, A.; Marci, G.; Palmisano, L.; Schiavello, M.; Uosaki, K.; Ikeda, S.; Ohtani, B. *J. Phys. Chem. B* **2002**, *106*, 637–645.
- (40) Di Paola, A.; García-López, E.; Ikeda, S.; Marci, G.; Ohtani, B.; Palmisano, L. *Catal. Today* **2002**, *75*, 87–93.
- (41) Dvoranová, D.; Brezová, V.; Mazúr, M.; Malati, M. A. *Appl. Catal. B Environ.* **2002**, *37*, 91–105.
- (42) Rao, K. V. K.; Naidu, S. V. N.; Iyengar, L. *J. Am. Ceram. Soc.* **1970**, *53*, 124–126.
- (43) Straumanis, M. E.; Ejima, T.; James, W. J. *Acta Crystallogr.* **1961**, *14*, 493–497.
- (44) *Handbook of Minerals Raman Spectra*; Laboratoire de géologie de Lyon ENS-Lyon France.
- (45) Chessin, H.; Hamilton, W. C.; Post, B. *Acta Crystallogr.* **1965**, *18*, 689–693.